

## **Response to Reviewer Comments**

Authors' responses inserted as blue text.

I find that the authors have revised their manuscript to satisfy the reviewer comments and I recommend that the paper be accepted in its current form, subject to one minor comment. The phrase added to the abstract (p. 1, lines 2-3) to address one of the reviewer comments now makes the sentence confusing. I see two separate issues in the determining of trends when fractal scaling is present: 1) the presence of fractal scaling has the potential to lead to false inference about the statistical significance of trends, and 2) the abundance of irregularly spaced data in water-quality monitoring networks complicates the ability to quantify fractal scaling and identify trends. Please revise the abstract to reflect these two points. I think that will help improve the readability of the abstract especially with respect to lines 2-3.

Response: Thank you very much for your review of this manuscript. We are glad to hear that our revisions have improved the manuscript. We have revised the manuscript based on your comment. Please see the revised sentence in Abstract. For your convenience, this revised sentence is pasted below:

*Fractal scaling presents challenges to the identification of deterministic trends because (1) fractal scaling has the potential to lead to false inference about the statistical significance of trends and (2) the abundance of irregularly spaced data in water quality monitoring networks complicates efforts to quantify fractal scaling.*

## **Notes to Editor**

Dear Editor,

Thank you again for handling this manuscript. In this revision, we have revised the manuscript based on the reviewer's suggestion.

In addition, we have also proofread the manuscript again and made a few grammatical revisions. These changes are marked in the "tracked change" version.

We hope that you will find it suitable for publication now.

Sincerely,

Qian

# Evaluation of statistical methods for quantifying fractal scaling in water quality time series with irregular sampling

Qian Zhang<sup>1</sup>, Ciaran J. Harman<sup>2</sup>, James W. Kirchner<sup>3,4,5</sup>

<sup>1</sup> University of Maryland Center for Environmental Science at the US Environmental Protection Agency Chesapeake Bay Program Office, 410 Severn Avenue, Suite 112, Annapolis, MD 21403 (formerly, Department of Geography and Environmental Engineering, Johns Hopkins University, 3400 North Charles Street, Baltimore, Maryland 21218)

<sup>2</sup> Department of Environmental Health and Engineering, Johns Hopkins University, 3400 North Charles Street, Baltimore, Maryland 21218

<sup>3</sup> Department of Environmental System Sciences, ETH Zurich, Universitätstrasse 16, CH-8092 Zurich, Switzerland

<sup>4</sup> Swiss Federal Research Institute WSL, Zürcherstrasse 111, CH-8903 Birmensdorf, Switzerland

<sup>5</sup> Department of Earth and Planetary Science, University of California, Berkeley, California 94720

Correspondence to: Qian Zhang ([qzhang@chesapeakebay.net](mailto:qzhang@chesapeakebay.net))

1 **Abstract.** River water-quality time series often exhibit fractal scaling, which here refers to  
2 autocorrelation that decays as a power law over some range of scales. Fractal scaling presents  
3 challenges to the identification of deterministic trends because (1) fractal scaling has the  
4 potential to lead to false inference about the statistical significance of trends and (2) the  
5 abundance of irregularly spaced data in water quality monitoring networks complicates efforts to  
6 quantify fractal scaling to avoid false inference on the statistical significance of trends. In the  
7 latter regard, but traditional methods for estimating fractal scaling -- in the form of spectral  
8 slope ( $\beta$ ) or other equivalent scaling parameters (*e.g.*, Hurst exponent) -- are generally  
9 inapplicable to irregularly sampled data. Here we consider two types of estimation approaches  
10 for irregularly sampled data and evaluate their performance using synthetic time series. These  
11 time series were generated such that (1) they exhibit a wide range of prescribed fractal scaling  
12 behaviors, ranging from white noise ( $\beta = 0$ ) to Brown noise ( $\beta = 2$ ), and (2) their sampling gap  
13 intervals mimic the sampling irregularity (as quantified by both the skewness and mean of gap-  
14 interval lengths) in real water-quality data. The results suggest that none of the existing methods  
15 fully account for the effects of sampling irregularity on  $\beta$  estimation. First, the results illustrate

16 the danger of using interpolation for ~~gap-gap~~-filling when examining auto-correlation, as the  
17 interpolation methods consistently under-estimate or over-estimate  $\beta$  under a wide range of  
18 prescribed  $\beta$  values and gap distributions. Second, the ~~long-established~~widely used Lomb-  
19 Scargle spectral method also consistently under-estimates  $\beta$ . A previously-published modified  
20 form, using only the lowest 5% of the frequencies for spectral slope estimation, has very poor  
21 precision, although the overall bias is small. Third, a recent wavelet-based method, coupled with  
22 an aliasing filter, generally has the smallest bias and root-mean-squared error among all methods  
23 for a wide range of prescribed  $\beta$  values and gap distributions. The aliasing method, however,  
24 does not itself account for sampling irregularity, and this introduces some bias in the result.  
25 Nonetheless, the wavelet method is recommended for estimating  $\beta$  in irregular time series until  
26 improved methods are developed. Finally, all methods' performances depend strongly on the  
27 sampling irregularity, highlighting that the accuracy and precision of each method are data-  
28 specific. Accurately quantifying the strength of fractal scaling in irregular water-quality time  
29 series remains an unresolved challenge for the hydrologic community and for other disciplines  
30 that must grapple with irregular sampling.

## 31 **Key Words**

32 Fractal scaling, autocorrelation, Hurst effect, river water-quality sampling, sampling irregularity,  
33 trend analysis

## 34 **1. Introduction**

### 35 *1.1. Autocorrelations in Time Series*

36 It is well known that time series from natural systems often exhibit auto-correlation, that is,  
37 observations at each time step are correlated with observations one or more time steps in the past.  
38 This property is usually characterized by the autocorrelation function (ACF), which is defined as  
39 follows for a process  $X_t$  at lag  $k$ :

$$\gamma(k) = cov(X_t, X_{t+k}) \quad (1)$$

40 In practice, auto-correlation has been frequently modeled with classical techniques such as auto-  
41 regressive (AR) or auto-regressive moving-average (ARMA) models (Darken *et al.*, 2002; Yue

42 *et al.*, 2002; Box *et al.*, 2008). These models assume that the underlying process has short-term  
43 memory, *i.e.*, the ACF decays exponentially with lag  $k$  (Box *et al.*, 2008).

44 Although the short-term memory assumption holds sometimes, it cannot adequately describe  
45 many time series whose ACFs decay as a power law (thus much slower than exponentially) and  
46 may not reach zero even for large lags, which implies that the ACF is non-summable. This  
47 property is commonly referred to as long-term memory or fractal scaling, as opposed to short-  
48 term memory (Beran, 2010).

49 Fractal scaling has been increasingly recognized in studies of hydrological time series,  
50 particularly for the common task of trend identification. Such hydrological series include river  
51 flows (Montanari *et al.*, 2000; Khaliq *et al.*, 2008; Khaliq *et al.*, 2009; Ehsanzadeh and  
52 Adamowski, 2010), air and sea temperatures (Fatichi *et al.*, 2009; Lennartz and Bunde, 2009;  
53 Franzke, 2012b; Franzke, 2012a), conservative tracers (Kirchner *et al.*, 2000; Kirchner *et al.*,  
54 2001; Godsey *et al.*, 2010), and non-conservative chemical constituents (Kirchner and Neal,  
55 2013; Aubert *et al.*, 2014). Because for fractal scaling processes the variance of the sample mean  
56 converges to zero much slower than the rate of  $n^{-1}$  ( $n$ : sample size), the fractal scaling property  
57 must be taken into account to avoid "false positives" (Type I errors) when inferring the statistical  
58 significance of trends (Cohn and Lins, 2005; Fatichi *et al.*, 2009; Ehsanzadeh and Adamowski,  
59 2010; Franzke, 2012a). Unfortunately, as stressed by Cohn and Lins (2005), it is "surprising that  
60 nearly every assessment of trend significance in geophysical variables published during the past  
61 few decades has failed [to do so]", and a similar tendency is evident in the decade following that  
62 statement as well.

### 63 ***1.2. Overview of Approaches for Quantification of Fractal Scaling***

64 Several equivalent metrics can be used to quantify fractal scaling. Here we provide a review  
65 of the definitions of such processes and several typical modeling approaches, including both  
66 time-domain and frequency-domain techniques, with special attention to their reconciliation. For  
67 a more comprehensive review, readers are referred to Beran *et al.* (2013), Boutahar *et al.* (2007),  
68 and Witt and Malamud (2013).

69 Strictly speaking,  $X_t$  is called a stationary long-memory process if the condition

$$\lim_{k \rightarrow \infty} k^\alpha \gamma(k) = C_1 > 0 \quad (2)$$

70 where  $C_1$  is a constant, is satisfied by some  $\alpha \in (0,1)$  (Boutahar *et al.*, 2007; Beran *et al.*, 2013).  
 71 Equivalently,  $X_t$  is a long-memory process if, in the spectral domain, the condition

$$\lim_{\omega \rightarrow 0} |\omega|^\beta f(\omega) = C_2 > 0 \quad (3)$$

72 is satisfied by some  $\beta \in (0,1)$ , where  $C_2$  is a constant and  $f(\omega)$  is the spectral density function  
 73 of  $X_t$ , which is related to ACF as follows (which is also known as the Wiener-Khinchin theorem):

$$f(\omega) = \frac{1}{2\pi} \sum_{k=-\infty}^{\infty} \gamma(k) e^{-ik\omega} \quad (4)$$

74 where  $\omega$  is angular frequency (Boutahar *et al.*, 2007).

75 One popular model for describing long-memory processes is the so-called fractional auto-  
 76 regressive integrated moving-average model, or ARFIMA  $(p, q, d)$ , which is an extension of  
 77 ARMA models and is defined as follows:

$$(1 - B)^d \varphi(B) X_t = \psi(B) \varepsilon_t \quad (5)$$

78 where  $\varepsilon_t$  is a series of independent, identically distributed Gaussian random numbers  $\sim (0, \sigma_\varepsilon^2)$ ,  
 79  $B$  is the backshift operator (*i.e.*,  $BX_t = X_{t-1}$ ), and functions  $\varphi(\cdot)$  and  $\psi(\cdot)$  are polynomials of order  
 80  $p$  and  $q$ , respectively. The fractional differencing parameter  $d$  is related to the parameter  $\alpha$  in Eq.  
 81 (2) as follows:

$$d = \frac{1 - \alpha}{2} \in (-0.5, 0.5) \quad (6)$$

82 (Beran *et al.*, 2013; Witt and Malamud, 2013).

83 In addition to a slowly decaying ACF, a long-memory process manifests itself in two other  
 84 equivalent fashions. One is the so-called ‘‘Hurst effect’’, which states that, on a log-log scale, the  
 85 range of variability of a process changes linearly with the length of the time period under  
 86 consideration. This power-law slope is often referred to as the ‘‘Hurst exponent’’ or ‘‘Hurst  
 87 coefficient’’  $H$  (Hurst, 1951), which is related to  $d$  as follows:

$$H = d + 0.5 \quad (7)$$

88 (Beran *et al.*, 2013; Witt and Malamud, 2013). The second equivalent description of long-  
 89 memory processes, this time from a frequency-domain perspective, is ‘‘fractal scaling’’, which  
 90 describes a power-law decrease in spectral power with increasing frequency, yielding power  
 91 spectra that are linear on log-log axes (Lomb, 1976; Scargle, 1982; Kirchner, 2005).

92 Mathematically, this inverse proportionality can be expressed as:

$$f(\omega) = C_3 |\omega|^{-\beta} \quad (8)$$

93 where  $C_3$  is a constant and the scaling exponent  $\beta$  is termed the “spectral slope.” In particular, for  
 94 spectral slopes of zero, one, and two, the underlying processes are termed as “white”, “pink” (or  
 95 “flicker”), and “Brown” (or “red”) noises, respectively (Witt and Malamud, 2013). Illustrative  
 96 examples of these three noises are shown in **Figure 1a-1c**.

97 In addition, it can be shown that the spectral density function for ARFIMA ( $p,d,q$ ) is

$$f(\omega) = \frac{\sigma_\varepsilon^2 |\psi(e^{-i\omega})|^2}{2\pi |\varphi(e^{-i\omega})|^2} |1 - e^{-i\omega}|^{-2d} \quad (9)$$

98 for  $-\pi < \omega < \pi$  (Boutahar *et al.*, 2007; Beran *et al.*, 2013). For  $|\omega| \ll 1$ , Eq. (9) can be  
 99 approximated by:

$$f(\omega) = C_4 |\omega|^{-2d} \quad (10)$$

100 with

$$C_4 = \frac{\sigma_\varepsilon^2 |\psi(1)|^2}{2\pi |\varphi(1)|^2} \quad (11)$$

101 Eq. (10) thus exhibits the asymptotic behavior required for a long-memory process given by Eq.  
 102 (3). In addition, a comparison of Eq. (10) and (8) reveals that,

$$\beta = 2d \quad (12)$$

103 Overall, these derivations indicate that these different types of scaling parameters (*i.e.*,  $\alpha$ ,  $d$ , and  
 104  $H$  and  $\beta$ ) can be used equivalently to describe the strength of fractal scaling. Specifically, their  
 105 equivalency can be summarized as follows:

$$\beta = 2d = 1 - \alpha = 2H - 1 \quad (13)$$

106 It should be noted, however, that the parameters  $d$ ,  $\alpha$ , and  $H$  are only applicable over a fixed  
 107 range of fractal scaling, which is equivalent to  $(-1, 1)$  in terms of  $\beta$ .

### 108 ***1.3. Motivation and Objective of this Work***

109 To account for fractal scaling in trend analysis, one must be able to first quantify the strength  
 110 of fractal scaling for a given time series. Numerous estimation methods have been developed for  
 111 this purpose, including Hurst rescaled range analysis, Higuchi’s method, Geweke and Porter-  
 112 Hudak’s method, Whittle’s maximum likelihood estimator, detrended fluctuation analysis, and  
 113 others (Taqqu *et al.*, 1995; Montanari *et al.*, 1997; Montanari *et al.*, 1999; Rea *et al.*, 2009;  
 114 Stroe-Kunold *et al.*, 2009). For brevity, these methods are not elaborated here; readers are  
 115 referred to Beran (2010) and Witt and Malamud (2013) for details. While these estimation

116 methods have been extensively adopted, they are unfortunately only applicable to regular (*i.e.*,  
117 evenly spaced) data, *e.g.*, daily streamflow discharge, monthly temperature, *etc.* In practice,  
118 many types of hydrological data, including river water-quality data, are often sampled irregularly  
119 or have missing values, and hence their strengths of fractal scaling cannot be readily estimated  
120 with the above traditional estimation methods.

121 Thus, estimation of fractal scaling in irregularly sampled data is an important challenge for  
122 hydrologists and practitioners. Many data analysts may be tempted to interpolate the time series  
123 to make it regular and hence analyzable (Graham, 2009). Although technically convenient,  
124 interpolation can be problematic if it distorts the series' autocorrelation structure (Kirchner and  
125 Weil, 1998). In this regard, it is important to evaluate various types of interpolation methods  
126 using carefully designed benchmark tests and to identify the scenarios under which the  
127 interpolated data can yield reliable (or, alternatively, biased) estimates of spectral slope.

128 Moreover, quantification of fractal scaling in real-world water-quality data is subject to  
129 several common complexities. First, water-quality data are rarely normally distributed; instead,  
130 they are typically characterized by log-normal or other skewed distributions (Hirsch *et al.*, 1991;  
131 Helsel and Hirsch, 2002), with potential consequences for  $\beta$  estimation. Moreover, water-quality  
132 data also tend to exhibit long-term trends, seasonality, and flow-dependence (Hirsch *et al.*, 1991;  
133 Helsel and Hirsch, 2002), which can also affect the accuracy of  $\beta$  estimates. Thus, it may be  
134 more plausible to quantify  $\beta$  in transformed time series after accounting for the seasonal patterns  
135 and discharge-driven variations in the original time series, which is ~~also~~ the approach taken in  
136 this [workpaper](#). For the trend aspect, however, it remains a puzzle whether the data set should be  
137 de-trended before conducting  $\beta$  estimation. Such de-trending treatment can certainly affect the  
138 estimated value of  $\beta$  and hence the validity of (or confidence in) any inference made regarding  
139 the statistical significance of temporal trends in the time series. This somewhat circular issue is  
140 beyond the scope of our current work -- it has been previously discussed in the context of short-  
141 term memory (Zetterqvist, 1991; Darken *et al.*, 2002; Yue *et al.*, 2002; Noguchi *et al.*, 2011;  
142 Clarke, 2013; Sang *et al.*, 2014), but it is not well understood in the context of fractal scaling (or  
143 long-term memory) and hence presents an important area for future research.

144 In the above context, the main objective of this work was to use Monte Carlo simulation to  
145 systematically evaluate and compare two broad types of approaches for estimating the strength

146 of fractal scaling (*i.e.*, spectral slope  $\beta$ ) in irregularly sampled river water-quality time series.

147 Specific aims of this work include the following:

148 (1) To examine the sampling irregularity of typical river water-quality monitoring data and  
149 to simulate time series that contain such irregularity; and

150 (2) To evaluate two broad types of approaches for estimating  $\beta$  in simulated irregularly  
151 sampled time series.

152 The first type of approach includes several forms of interpolation techniques for gap filling, thus  
153 making the data regular and analyzable by traditional estimation methods. The second type of  
154 approach includes the well-known Lomb-Scargle periodogram (Lomb, 1976; Scargle, 1982) and  
155 a recently developed wavelet method combined with a spectral aliasing filter (Kirchner and Neal,  
156 2013). The latter two methods can be directly applied to irregularly spaced data; here we aim to  
157 compare them with the interpolation techniques. Details of these various approaches are  
158 provided in **Section 3.1**.

159 This work was designed to make several specific contributions. First, it uses benchmark tests  
160 to quantify the performance of a wide range of methods for estimating fractal scaling in  
161 irregularly sampled water-quality data. Second, it proposes an innovative and general approach  
162 for modeling sampling irregularity in water-quality records. Third, while this work was not  
163 intended to compare all published estimation methods for fractal scaling, it does provide and  
164 demonstrate a generalizable framework for data simulation (with gaps) and  $\beta$  estimation, which  
165 can be readily applied toward the evaluation of other methods that are not covered here. Last but  
166 not least, while this work was intended to help hydrologists and practitioners understand the  
167 performance of various approaches for water-quality time series, the findings and approaches  
168 may be broadly applicable to irregularly sampled data in ~~many~~ other scientific disciplines.

169 The rest of the paper is organized as follows. We propose a general approach for modeling  
170 sampling irregularity in typical river water-quality data and discuss our approach for simulating  
171 irregularly sampled data (**Section 2**). We then introduce the various methods for estimating  
172 fractal scaling in irregular time series and compare their estimation performance (**Section 3**). We  
173 close with a discussion of the results and implications (**Section 4**).



## 174 2. Quantification of Sampling Irregularity in River Water-Quality Data

### 175 2.1. Modeling of Sampling Irregularity

176 River water-quality data are often sampled irregularly. In some cases, samples are taken  
177 more frequently during particular periods of interest, such as high flows or drought periods; here  
178 we will address the implications of the irregularity, but not the (intentional) bias, inherent in such  
179 a sampling strategy. In other cases, the sampling is planned with a fixed sampling interval (*e.g.*,  
180 1 day) but samples are missed (or lost, or fail quality-control checks) at some time steps during  
181 implementation. In still other cases, the sampling is intrinsically irregular because, for example,  
182 one cannot measure the chemistry of rainfall on rainless days or the chemistry of a stream that  
183 has dried up. Theoretically, any deviation from fixed-interval sampling can affect the subsequent  
184 analysis of the time series.

185 To quantify the sampling irregularity, we propose a simple and general approach that can be  
186 applied to any time series of monitoring data. Specifically, for a given time series with  $N$  points,  
187 the time intervals between adjacent samples are calculated; these intervals themselves make up a  
188 time series of  $N-1$  points that we call  $\Delta t$ . In addition, the following parameters are calculated to  
189 quantify its sampling irregularity:

- 190 •  $L$  = the length of the period of record,
- 191 •  $N$  = the number of samples in the record,
- 192 •  $\Delta t_{nominal}$  = the nominal sampling interval under regular sampling (*e.g.*,  $\Delta t_{nominal} = 1$  day  
193 for daily samples),
- 194 •  $\Delta t^* = \Delta t / \Delta t_{nominal}$ , the sample intervals non-dimensionalized by the nominal sampling  
195 interval,
- 196 •  $\Delta t_{average} = L / (N - 1)$  the average of all the entries in  $\Delta t$ .

197 The quantification is illustrated with two simple examples. The first example contains data  
198 sampled every hour from 1:00 am to 11:00 am on one day. In this case,  $L = 10$  hours,  $N = 11$   
199 samples,  $\Delta t = \{1, 1, 1, 1, 1, 1, 1, 1, 1, 1\}$  hour, and  $\Delta t_{nominal} = \Delta t_{average} = 1$  hour. The second  
200 example contains data sampled at 1:00 am, 3:00 am, 4:00 am, 8:00 am, and 11:00 am. In this  
201 case,  $L = 10$  hours,  $N = 5$  samples,  $\Delta t = \{2, 1, 4, 3\}$  hours,  $\Delta t_{nominal} = 1$  hour, and  $\Delta t_{average} = 2.5$   
202 hours. It is readily evident that the first case corresponds to fixed-interval (regular) sampling that

203 has the property of  $\Delta t_{average}/\Delta t_{nominal} = 1$  (dimensionless), whereas the second case corresponds to  
204 irregular sampling for which  $\Delta t_{average}/\Delta t_{nominal} > 1$ .

205 The dimensionless set  $\Delta t^*$  contains essential information for determining sampling  
206 irregularity. This set is modeled as independent, identically distributed values drawn from a  
207 negative binomial (NB) distribution. This distribution has two dimensionless parameters, the  
208 shape parameter ( $\lambda$ ) and the mean parameter ( $\mu$ ), which collectively represent the irregularity of  
209 the samples. The NB distribution is a flexible distribution that provides a discrete analogue of a  
210 gamma distribution. The geometric distribution, itself the discrete analogue of the exponential  
211 distribution, is a special case of the NB distribution when  $\lambda = 1$ .

212 The parameters  $\mu$  and  $\lambda$  represent different aspects of sampling irregularity, as illustrated by  
213 the examples shown in **Figure 2**. The mean parameter  $\mu$  represents the fractional increase in the  
214 average interval between samples due to gaps:  $\mu = \text{mean}(\Delta t^*) - 1 = (\Delta t_{average} - \Delta t_{nominal})/\Delta t_{nominal}$ .  
215 Thus the special case of  $\mu = 0$  corresponds to regular sampling (*i.e.*,  $\Delta t_{average} = \Delta t_{nominal}$ ), whereas  
216 any larger value of  $\mu$  corresponds to irregular sampling (*i.e.*,  $\Delta t_{average} > \Delta t_{nominal}$ ) (**Figure 2c**). The  
217 shape parameter  $\lambda$  characterizes the similarity of gaps to each other; that is, a small  $\lambda$  indicates  
218 that the samples contain gaps of widely varying lengths, whereas a large  $\lambda$  indicates that the  
219 samples contain many gaps of similar lengths (**Figure 2a-2b**).

220 To visually illustrate these gap distributions, representative samples of irregular time series  
221 are presented in **Figure 1** for the three special processes described above (**Section 1.2**), *i.e.*,  
222 white noise, pink noise, and Brown noise. Specifically, three different gap distributions, namely,  
223  $\text{NB}(\lambda = 1, \mu = 1)$ ,  $\text{NB}(\lambda = 1, \mu = 14)$ , and  $\text{NB}(\lambda = 0.01, \mu = 1)$ , were simulated and each was  
224 applied to convert the three original (regular) time series (**Figure 1a-1c**) to irregular time series  
225 (**Figure 1d-1f**). These simulations clearly illustrate the effects of the two parameters  $\lambda$  and  $\mu$ . In  
226 particular, compared with  $\text{NB}(\lambda = 1, \mu = 1)$ ,  $\text{NB}(\lambda = 1, \mu = 14)$  shows a similar level of sampling  
227 irregularity (same  $\lambda$ ) but a much longer average gap interval (larger  $\mu$ ). Again compared with  
228  $\text{NB}(\lambda = 1, \mu = 1)$ ,  $\text{NB}(\lambda = 0.01, \mu = 1)$  shows the same average interval (same  $\mu$ ) but a much more  
229 irregular (skewed) gap distribution that contains a few very large gaps (smaller  $\lambda$ ).

## 230 **2.2. Examination of Sampling Irregularity in Real River Water-Quality Data**

231 The above modeling approach was applied to real water-quality data from two large river  
232 monitoring networks in the United States to examine sampling irregularity. One such network is  
233 the Chesapeake Bay River Input Monitoring program, which typically samples streams bi-

234 monthly to monthly, accompanied with additional sampling during stormflows (Langland *et al.*,  
235 2012; Zhang *et al.*, 2015). These data were obtained from the U.S. Geological Survey National  
236 Water Information System (<http://doi.org/10.5066/F7P55KJN>). The other network is the Lake  
237 Erie and Ohio tributary monitoring program, which typically samples streams at a daily  
238 resolution (National Center for Water Quality Research, 2015). For each site, we determined the  
239 NB parameters to quantify sampling irregularity. The mean parameter  $\mu$  can be estimated as  
240 described above, and the shape parameter  $\lambda$  can be calculated directly from the mean and  
241 variance of  $\Delta t^*$  as follows:  $\lambda = \mu^2 / [\text{var}(\Delta t^*) - \mu] = (\text{mean}(\Delta t^*) - 1)^2 / [\text{var}(\Delta t^*) - \text{mean}(\Delta t^*) + 1]$ .  
242 Alternatively, a maximum likelihood approach can be used, which employs the “*fitdist*” function  
243 in the “*fitdistrplus*” R package (Delignette-Muller and Dutang, 2015). In general, the two  
244 approaches ~~have produced~~ similar results, which are summarized in **Table 1**, with two examples  
245 of fitted NB distributions shown in **Figure 3**.

246 For the Chesapeake Bay River Input Monitoring program (9 sites), total nitrogen (TN) and  
247 total phosphorus (TP) are taken as representatives of water-quality constituents. According to the  
248 maximum likelihood approach, the shape parameter  $\lambda$  varies between 0.7 and 1.2 for TN and  
249 between 0.8 and 1.1 for TP (**Table 1**). These  $\lambda$  values are around 1.0, reflecting the fact that  
250 these sites have relatively even gap distributions (*i.e.*, relatively balanced counts of large and  
251 small gaps). The mean parameter  $\mu$  varies between 9.5 and 19.6 for TN and between 13.4 and  
252 24.4 for TP in the Chesapeake monitoring network, corresponding to  $\Delta t_{\text{average}}$  of 10.5–20.6 days  
253 for TN and 14.4–25.4 days for TP, respectively. This is consistent with the fact that these sites  
254 have typically been sampled bi-monthly to monthly, along with additional sampling during  
255 stormflows (Langland *et al.*, 2012; Zhang *et al.*, 2015).

256 For the Lake Erie and Ohio tributary monitoring program (6 sites), ~~the records~~ of nitrate-  
257 plus-nitrite (NO<sub>x</sub>) and TP were examined. According to the maximum likelihood approach, the  
258 shape parameter  $\lambda$  is approximately 0.01 for both constituents (**Table 1**). These very low  $\lambda$  values  
259 occur because these time series contain a few very large gaps, ranging from 35 days to 1109  
260 days (~3 years). The mean parameter  $\mu$  varies between 0.06 and 0.22, corresponding to  $\Delta t_{\text{average}}$   
261 of 1.06 and 1.22 days, respectively. This is consistent with fact that these sites have been  
262 sampled at a daily resolution with occasional missing values on some days (Zhang and Ball,  
263 2017).

### 264 2.3. Simulation of Time Series with Irregular Sampling

265 To evaluate the various  $\beta$  estimation methods, our first step was to use Monte Carlo  
266 simulation to produce time series that mimic the sampling irregularity observed in real water-  
267 quality monitoring data. We began by simulating regular (gap free) time series using the  
268 fractional noise simulation method of Witt and Malamud (2013), which is based on inverse  
269 Fourier filtering of white noises. Our analysis showed this method performed reasonably well  
270 compared to other simulation methods for  $\beta$  values between 0 and 1 (see Supporting Information  
271 S1). In addition, this method can also simulate  $\beta$  values beyond this range. The noises simulated  
272 by the Witt and Malamud method, however, are band-limited to the Nyquist frequency (half of  
273 the sampling frequency) of the underlying white noise time series, whereas true fractional noises  
274 would contain spectral power at all frequencies, extending well above the Nyquist frequency for  
275 any sampling. Thus these band-limited noises will be less susceptible to spectral aliasing than  
276 true fractional noises would be; see Kirchner (2005) for detailed discussions of the aliasing issue.

277 100 replicates of regular (gap free) time series were produced for nine prescribed spectral  
278 slopes, which vary from  $\beta = 0$  (white noise) to  $\beta = 2$  (Brownian motion or “random walk”) with  
279 an increment of 0.25 (*i.e.*, 0, 0.25, 0.5, 0.75, 1.0, 1.25, 1.5, 1.75, and 2). These regular time series  
280 each have a length ( $N$ ) of 9125, which can be interpreted as 25 years of regular daily samples  
281 (that is,  $\Delta t_{nominal} = 1$  day).

282 ~~Each of the~~The simulated regular time series ~~was~~were converted to irregular time series using  
283 gap intervals that were simulated with NB distributions. To make these gap intervals mimic  
284 those in typical river water-quality time series, representative NB parameters were chosen based  
285 on results from **Section 2.2**. Specifically,  $\mu$  was set at 1 and 14, corresponding to  $\Delta t_{average}$  of 2  
286 days and 15 days respectively. For  $\lambda$ , we chose four values that span three orders of magnitude,  
287 *i.e.*, 0.001, 0.1, 1, and 10. Note that when  $\lambda = 1$  the generated time series corresponds to a  
288 Bernoulli process. With the chosen values of  $\mu$  and  $\lambda$ , a total of eight scenarios were generated,  
289 which were implemented using the “*rnbinom*” function in the “*stats*” R package (R Development  
290 Core Team, 2014):

- 291 1)  $\mu = 1$  (*i.e.*,  $\Delta t_{average}/\Delta t_{nominal} = 2$ ),  $\lambda = 0.01$ ,
- 292 2)  $\mu = 1$ ,  $\lambda = 0.1$ ,
- 293 3)  $\mu = 1$ ,  $\lambda = 1$ ,
- 294 4)  $\mu = 1$ ,  $\lambda = 10$ ,

- 295 5)  $\mu = 14$  (i.e.,  $\Delta t_{average} / \Delta t_{nominal} = 15$ ),  $\lambda = 0.01$ ,  
 296 6)  $\mu = 14$ ,  $\lambda = 0.1$ ,  
 297 7)  $\mu = 14$ ,  $\lambda = 1$ ,  
 298 8)  $\mu = 14$ ,  $\lambda = 10$ .

299 Examples of these simulations are shown with boxplots in **Figure 2**.

### 300 **3. Evaluation of Proposed Estimation Methods for Irregular Time Series**

#### 301 **3.1. Summary of Estimation Methods**

302 For the simulated irregular time series,  $\beta$  was estimated using the aforementioned two types  
 303 of approaches. The first type includes 11 different interpolation methods (designated as B1-B11  
 304 below) to fill the data gaps, thus making the data regular and analyzable by traditional methods:

- 305 B1) Global mean: all missing values replaced with the mean of all observations;  
 306 B2) Global median: all missing values replaced with the median of all observations;  
 307 B3) Random replacement: all missing values replaced with observations randomly drawn  
 308 (with replacement) from the time series;  
 309 B4) Next observation carried backward: each missing value replaced with the next available  
 310 observation;  
 311 B5) Last observation carried forward: each missing value replaced with the preceding  
 312 available observation;  
 313 B6) Average of the two nearest samples: ~~it replaces~~ each missing value replaced with the  
 314 mean of its next and preceding available observations;  
 315 B7) Lowess (locally weighted scatterplot smoothing) with a smoothing span of 1: missing  
 316 values replaced using fitted values from a lowess model determined using all available  
 317 observations (Cleveland, 1981);  
 318 B8) Lowess with a smoothing span of 0.75: same as B7 except that the smoothing span is 75%  
 319 of the available data (similar distinction follows for B9-B11);  
 320 B9) Lowess with a smoothing span of 50%;  
 321 B10) Lowess with a smoothing span of 30%; and  
 322 B11) Lowess with a smoothing span of 10%.

323 B4 and B5 were implemented using the “*na.locf*” function in the “*zoo*” R package (Zeileis and  
 324 Grothendieck, 2005). B7-B11 were implemented using the “*loess*” function in the “*stats*” R

325 package (R Development Core Team, 2014). An illustration of these interpolation methods is  
326 provided in **Figure 4**. The interpolated data, along with the original regular data (designated as  
327 A1) were analyzed using the Whittle’s maximum likelihood method for  $\beta$  estimation, which was  
328 implemented using the “*FDWhittle*” function in the “*fractal*” R package (Constantine and  
329 Percival, 2014).

330 The second type of approaches estimates  $\beta$  directly from ~~in~~ the irregularly sampled data  
331 directly, using several variants of the Lomb-Scargle periodogram (designated as C1a-C1c below),  
332 and a recently developed wavelet-based method (designated as C2 below). Specifically, these  
333 approaches are:

334 C1a) Lomb-Scargle periodogram: the spectral density of the time series (with gaps) is  
335 estimated and the spectral slope is fit using all frequencies (Lomb, 1976; Scargle, 1982).  
336 This is a classic method for examining periodicity in irregularly sampled data, which is  
337 analogous to the more familiar fast Fourier transform method often used for regularly  
338 sampled data;

339 C1b) Lomb-Scargle periodogram with 5% data: same as C1a except that the fitting of the  
340 spectral slope considers only the lowest 5% of the frequencies (Montanari *et al.*, 1999);

341 C1c) Lomb-Scargle periodogram with “binned” data: same as C1a except that the fitting of  
342 the spectral slope is performed on binned data in three steps: (1) The entire range of  
343 frequency is divided into 100 equal-interval bins on logarithmic scale. (2) The  
344 respective medians of frequency and power spectral density are calculated for each of  
345 the 100 bins. (3) The 100 pairs of median frequency and median spectral density are  
346 used to estimate the spectral slope on a log-log scale.

347 C2) Kirchner and Neal (2013)’s wavelet method: uses a modified version of Foster’s  
348 weighted wavelet spectrum (Foster, 1996) to suppress spectral leakage from low  
349 frequencies and applies an aliasing filter (Kirchner, 2005) to remove spectral aliasing  
350 artifacts at high frequencies.

351 C1a was implemented using the “*spec.ls*” function in the “*cts*” R package (Wang, 2013). C2 was  
352 run in *C*, using codes modified from those in Kirchner and Neal (2013).

### 353 **3.2. Evaluation of Methods’ Performance**

354 Each estimation method listed above was applied to the simulated data (**Section 2.3**) to  
355 estimate  $\beta$ , which were then compared with the prescribed (“true”)  $\beta$  to quantify the performance

356 of each method. Plots of method evaluation for all simulations are provided as **Figures S3-S12**  
357 (Supporting Information S2). Close inspections of these plots reveal some general patterns of the  
358 methods' performance. For brevity, these patterns are presented with a subset of the plots, which  
359 correspond to the cases where true  $\beta = 1$  and shape parameter  $\lambda = 0.01, 0.1, 1, \text{ and } 10$  (**Figure 5**).  
360 In general,  $\beta$  values estimated using the regular data (A1) are very close to 1.0, which indicates  
361 that the adopted fractional noise generation method and the Whittle's maximum likelihood  
362 estimator have small combined simulation and estimation bias. This is perhaps unsurprising,  
363 since the estimator is based on the Fourier transform and the noise generator is based on an  
364 inverse Fourier transform; thus, one method is essentially just the inverse of the other. One  
365 should also note that when fractional noises are not arbitrarily band-limited at the Nyquist  
366 frequency (as they inherently are with the noise generator that is used here), spectral aliasing  
367 should lead to spectral slopes that are flatter than expected (Kirchner, 2005), and thus to  
368 underestimates of LRD.

369 For the simulated irregular data, the estimation methods differ widely in their performance.  
370 Specifically, three interpolation methods (*i.e.*, B4-B6) consistently over-estimate  $\beta$ , indicating  
371 that they introduce additional correlations into the time series, reducing its short-timescale  
372 variability. In contrast, the other eight interpolation methods (*i.e.*, B1-B3 and B7-B11) generally  
373 under-estimate  $\beta$ , indicating that the interpolated points are less correlated than the original time  
374 series, thus introducing additional variability on short timescales. As expected, results from the  
375 lowess methods (B7-B11) depend strongly on the size of smoothing window, that is, ~~more~~  
376 ~~severe under-estimation of  $\beta$  is~~ more severely under-estimated ~~produced~~ as the smoothing  
377 window becomes wider. In fact, when the smoothing window is 1.0 (*i.e.*, method B7), lowess  
378 performs the interpolation using all data available and thus behaves similarly to interpolations  
379 based on global means (B1) or global medians (B2), except that lowess fits a polynomial curve  
380 instead of constant values. However, whenever a sampling gap is much shorter than the  
381 smoothing window, the infilled lowess value will be close to the local mean or median, and the  
382 abrupt jumps produced by these infilled values will artificially increase the variance in the time  
383 series at high frequencies, leading to an artificially reduced spectral slope  $\beta$  and correspondingly,  
384 an underestimate of  $\beta$ . This mechanism explains why lowess interpolation distorts  $\beta$  more when  
385 there are many small gaps (large  $\lambda$ ), and therefore more jumps to, and away from, the infilled  
386 values, than when there are only a few large gaps (small  $\lambda$ ).

387 Among the direct methods (*i.e.*, C1a, C1b, C1c, and C2), the Lomb-Scargle method, with  
 388 original data (C1a) or binned data (C1c) tends to under-estimate  $\beta$ , though the underestimation  
 389 by C1c is generally less severe. The modified Lomb-Scargle method (C1b), using only the  
 390 lowest 5% of frequencies, yields estimates that are centered around 1.0. However, C1b has the  
 391 highest variability (*i.e.*, least precision) in  $\beta$  estimates among all methods. Compared with all the  
 392 above methods, the wavelet method (C2) has much better performance in terms of both accuracy  
 393 and precision when  $\lambda$  is 1 or 10, a slightly better performance when  $\lambda$  is 0.1, but a worse  
 394 performance when  $\lambda$  is 0.01.

395 The shape parameter  $\lambda$  greatly affects the performance of the estimation methods. All the  
 396 interpolation methods that under-estimate  $\beta$  (*i.e.*, B1-B3 and B7-B11) perform worse as  $\lambda$   
 397 increases from 0.01 to 10. This effect can be interpreted as follows: when the time series  
 398 contains a large number of relatively small gaps (*e.g.*,  $\lambda = 1$  or 10), there are many jumps (which,  
 399 as noted above, contain mostly high-frequency variance) between the original data and the  
 400 infilled values, resulting in more severe under-estimation. In contrast, when the data contain only  
 401 a small number of very large gaps (*e.g.*,  $\lambda = 0.01$  or 0.1), there are fewer of these jumps, resulting  
 402 in minimal under-estimation. Similar effects of  $\lambda$  are also observed with the interpolation  
 403 methods that show over-estimation (*i.e.*, B4-B6) – that is, over-estimation is more severe when  $\lambda$   
 404 is larger. Similarly, the Lomb-Scargle method (C1a and C1c) performs worse (more serious  
 405 underestimation) as  $\lambda$  increases. Finally, method C2 seems to perform the best when  $\lambda$  is large (1  
 406 or 10), but not well when  $\lambda$  is very small (0.01), as noted above. This result highlights the  
 407 sensitivity of the wavelet method to the presence of a few large gaps in the time series. For such  
 408 cases, a potentially more feasible approach is to break the whole time series into several  
 409 segments (each without long gaps) and then apply the wavelet method (C2) to analyze each  
 410 segment separately. If this can yield more accurate estimates, then further simulation  
 411 experiments should be designed to systematically determine how long the gap needs to be to  
 412 invoke such an approach.

413 Next, the method evaluation is extended to all the simulated spectral slopes, that is,  $\beta = 0$ ,  
 414 0.25, 0.5, 0.75, 1.0, 1.25, 1.5, 1.75, and 2. For ease of discussion, three quantitative criteria were  
 415 proposed for evaluating performance, namely, bias (B), standard deviation (SD), and root-mean-  
 416 squared error (RMSE), as defined below:

$$B_i = \bar{\beta}_i - \beta_{true} \quad (14)$$



$$SD_i = \sqrt{\frac{1}{99} \sum_{j=1}^{100} (\beta_{i,j} - \bar{\beta}_i)^2} \quad (15)$$

$$RMSE_i = \sqrt{B_i^2 + SD_i^2} \quad (16)$$

417 where  $\bar{\beta}_i$  is the mean of 100  $\beta$  values estimated by method  $i$ , and  $\beta_{true}$  is the prescribed  $\beta$  value  
 418 for simulation of the initial regular time series. In general,  $B$  and  $SD$  can be considered as the  
 419 models' systematic error and random error, respectively, and  $RMSE$  serves as an integrated  
 420 measure of both errors. For all evaluations, plots of bias and  $RMSE$  are provided in the main text.  
 421 (Plots of  $SD$  are provided as **Figure S7** and **Figure S12** for simulations with  $\mu = 1$  and  $\mu = 14$ ,  
 422 respectively.)

423 For simulations with  $\mu = 1$ , results of estimation bias and  $RMSE$  are summarized in **Figure 6**  
 424 and **Figure 7**, respectively. (More details are provided in **Figures S3-S6**.) For brevity, we focus  
 425 on three direct methods (C1a, C1b and C2) and three representative interpolation methods.  
 426 (Specifically, B1 represents B1-B3 and B7; B6 represents B4-B6, and B8 represents B8-B11.)  
 427 Overall, these six methods show mixed performances. In terms of bias (**Figure 6**), B1 (global  
 428 mean) and B8 (lowess with a smoothing span of 0.75) tend to have negative bias, particularly for  
 429 time series with (1) moderate-to-large  $\beta_{true}$  values and (2) large  $\lambda$  values (*i.e.*, less skewed gap  
 430 intervals). By contrast, B1 and B8 generally have minimal bias when (1)  $\beta_{true}$  is close to zero (*i.e.*,  
 431 when the simulated time series is close to white noise); and (2)  $\lambda$  is small (*e.g.*, 0.01), since  
 432 interpolating a few large gaps cannot significantly affect the overall correlation structure. In  
 433 addition, lowess interpolation with a larger smoothing window tends to yield more negatively  
 434 biased estimates (data not shown). The other interpolation method, B6 (mean of the two nearest  
 435 neighbors) tends to over-estimate  $\beta$ , particularly for time series with (1) small  $\beta_{true}$  values and (2)  
 436 large  $\lambda$  values. At large  $\beta_{true}$  values (*e.g.*, 2.0), the auto-correlation is already very strong such  
 437 that taking the mean of two neighbors for gap filling does not introduce much additional  
 438 correlation, as opposed to the case of small  $\beta_{true}$  values. The Lomb-Scargle methods (C1a and  
 439 C1b) generally have negative bias, particularly for time series with (1) moderate-to-large  $\beta_{true}$   
 440 values (for both methods) and (2) large  $\lambda$  values (for C1a), which is similar to B1 and B8.  
 441 However, C1b overall shows less severe bias than C1a. Finally, the wavelet method (C2) shows  
 442 generally the smallest bias among all methods. However, its performance advantage is not as

443 great when the time series has small  $\lambda$  values (*i.e.*, very skewed gap intervals), as noted above,  
444 which may be due to the fact that the aliasing filter was designed for regular time series. In terms  
445 of SD (**Figure S7**), method C1b performs the worst among all methods (as noted above), method  
446 B6 and B8 perform poorly for large  $\beta_{true}$  values, and method C2 performs poorly for  $\beta_{true} = 0$ . In  
447 terms of RMSE (**Figure 7**), methods B1, B8, C1a, and C1b perform well for small  $\beta_{true}$  values  
448 and small  $\lambda$  values, whereas method B6 performs well for large  $\beta_{true}$  values and small  $\lambda$  values. In  
449 comparison, method C2 has the smallest RMSEs among all methods, and its RMSEs are  
450 similarly small for the wide range of  $\beta_{true}$  and  $\lambda$  values. In general, the wavelet method can be  
451 considered the best among all [the tested](#) methods.

452 For simulations with  $\mu = 14$ , results of estimation bias and RMSE are summarized in  
453 **Figure 8** and **Figure 9**, respectively. (More details are provided in **Figures S8-S11**.) Overall,  
454 these methods show mixed performances that are generally similar to the cases when  $\mu = 1$ , as  
455 discussed above. These results highlight the generality of these methods' performances, which  
456 applies at least to the range of  $\mu = [1, 14]$ . In addition, all methods show generally larger RMSE  
457 for  $\mu = 14$  than  $\mu = 1$ , indicating their dependence on the mean gap interval (**Figure 9**). Perhaps  
458 the most notable difference is observed with method C2, which in this case shows positive bias  
459 for small  $\lambda$  values (0.01 and 0.1) and negative bias for large  $\lambda$  values (1 and 10) (**Figure 8f**). It  
460 nonetheless generally shows the smallest RMSEs among all the tested methods.

### 461 **3.3. Quantification of Spectral Slopes in Real Water-Quality Data**

462 In this section, the proposed estimation approaches were applied to quantify  $\beta$  in real water-  
463 quality data from the two monitoring programs presented in **Section 2.2** (**Table 1**). As noted in  
464 **Section 1.3**, such real data are typically much more complex than our simulated time series,  
465 because of (1) strong deviations from normal distributions and (2) effects of flow-dependence,  
466 seasonality, and temporal trends (Hirsch *et al.*, 1991; Helsel and Hirsch, 2002). In this regard,  
467 future research may simulate time series with these important characteristics and evaluate the  
468 performance of various estimation approaches, perhaps following the modeling framework  
469 described here. Alternatively, one may quantify  $\beta$  in transformed time series after accounting  
470 for the above aspects. In this work, we have taken the latter approach for a preliminary  
471 investigation. Specifically, we have used the published Weighted Regressions on Time,  
472 Discharge, and Season (WRTDS) method (Hirsch *et al.*, 2010) to transform the original time

473 series. This widely accepted method estimates daily concentrations based on discretely collected  
474 concentration samples using time, season, and discharge as explanatory variables, *i.e.*,

$$\ln(C) = \beta_0 + \beta_1 t + \beta_2 \ln(Q) + \beta_3 \sin(2\pi t) + \beta_4 \cos(2\pi t) + \varepsilon \quad (17)$$

475 where  $C$  is concentration,  $Q$  is daily discharge,  $t$  is time in decimal years,  $\beta_i$  are fitted  
476 coefficients, and  $\varepsilon$  is the error term. The 2<sup>nd</sup> and 3<sup>rd</sup> terms on the right represent time and  
477 discharge effects, respectively, whereas the 4<sup>th</sup> and 5<sup>th</sup> terms collectively represent cyclical  
478 seasonal effects. For a full description of this method, see Hirsch *et al.* (2010). In this work,  
479 WRTDS was applied to obtain the time series of estimated daily concentrations for each  
480 constituent at each site. The difference between observed concentration ( $C_{obs}$ ) and estimated  
481 concentration ( $C_{est}$ ) was calculated in logarithmic space to obtain the concentration residuals,

$$residuals = \ln(C_{obs}) - \ln(C_{est}) \quad (18)$$

482 For our data sets, histograms of concentration residuals (expressed in natural log concentration  
483 units) are shown in **Figures S13-S16** (Supporting Information S3). Compared with the original  
484 concentration data, these model residuals are much more nearly normal and homoscedastic.  
485 Moreover, the model residuals are less susceptible to the issues of temporal, seasonal, and  
486 discharge-driven variations than the original concentrations. Therefore, the model residuals are  
487 more appropriate than the original concentrations for  $\beta$  estimation using the simulation  
488 framework adopted in this work.

489 The estimated  $\beta$  values for the concentration residuals are summarized in **Figure 10**. Clearly,  
490 the estimated  $\beta$  varies considerably with the estimation method. In addition, the estimated  $\beta$   
491 varies with site and constituent (*i.e.*, TP, TN, or NO<sub>x</sub>). Our discussion below focuses on the  
492 wavelet method (C2), because it is established above that this method performs better than the  
493 other estimation methods under a wide range of gap conditions. We emphasize that it is beyond  
494 our current scope to precisely quantify  $\beta$  in these water-quality data sets, but our simulation  
495 results presented above (**Section 3.2**) can be used as references to qualitatively evaluate the  
496 reliability of C2 and/or other methods for these data sets.

497 For TN and TP concentration data at the Chesapeake River Input Monitoring sites (**Table 1**),  
498  $\mu$  varies between 9.5 and 24.4, whereas  $\lambda$  is  $\sim 1.0$ . Thus, the simulated gap scenario of NB( $\mu = 14$ ,  
499  $\lambda = 1$ ) can be used as a reasonable reference to assess methods' reliability (**Figure 8**). Based on  
500 method C2, the estimated  $\beta$  ranges between  $\beta = 0.36$  and  $\beta = 0.61$  for TN and between  $\beta = 0.30$   
501 and  $\beta = 0.58$  for TP at these sites (**Figure 10**). For such ranges, the simulation results indicate

502 that method C2 tends to moderately under-estimate  $\beta$  under this gap scenario (**Figure 8**), and  
503 hence spectral slopes for TN and TP at these Chesapeake sites are likely probably slightly higher  
504 than those presented above.

505 For  $\text{NO}_x$  and TP concentration data at the Lake Erie and Ohio sites (**Table 1**),  $\mu$  varies  
506 between 0.06 and 0.22, whereas  $\lambda$  is  $\sim 0.01$ . Thus, the simulated gap scenario of NB( $\mu = 1$ ,  $\lambda =$   
507 0.01) can be used as a reasonable reference to assess the methods' reliability (**Figure 6**). For  
508 such small  $\lambda$  (*i.e.*, a few gaps that are very dissimilar from others), C2 is not reliable for  $\beta$   
509 estimation, as reflected by the generally positive bias in the simulation results. By contrast,  
510 methods B1 (interpolation with global mean) and B8 (lowess with span 0.75) both perform quite  
511 well under this gap scenario (**Figure 6**). These two methods provide almost identical  $\beta$  estimates  
512 for each site-constituent combination, ranging from  $\beta = 1.0$  to  $\beta = 1.5$  for  $\text{NO}_x$  and from  $\beta = 1.0$   
513 to  $\beta = 1.4$  for TP (**Figure 10**).

514 Overall, the above analysis of real water-quality data has illustrated the wide variability in  $\beta$   
515 estimates, with different choices of estimation methods yielding very different results. To our  
516 knowledge, these water-quality data have not heretofore previously been analyzed in this context.  
517 As illustrated above, our simulation experiments (**Section 3.2**) can be used as references to  
518 coarsely evaluate the reliability of each method under specific gap scenarios, thereby  
519 considerably narrowing the likely range of the estimated spectral slopes. Nonetheless, our results  
520 demonstrate that the analyzed water-quality time series can exhibit strong fractal scaling,  
521 particularly at the Lake Erie and Ohio tributary sites. Thus, an important implication is that  
522 researchers and analysts should be cautious when applying standard statistical methods to  
523 identify temporal trends in such water-quality data sets (Kirchner and Neal, 2013). In future  
524 work, one may consider applying Bayesian statistical analysis or other approaches to more  
525 accurately quantify the spectral slope and associated uncertainty for real water-quality data  
526 analysis. In addition, the modeling framework presented here ~~in~~ (including both gap simulation  
527 and  $\beta$  estimation) may be extended to simulations of irregular time series that have prescribed  
528 spectral slopes and also superimposed temporal trends, which can then be used to evaluate the  
529 validity of various statistical methods for identifying trends s and their associated statistical  
530 significance.

#### 531 4. Conclusions

532 River water-quality time series often exhibit fractal scaling behavior, which presents  
533 challenges to the identification of deterministic trends. Because traditional spectral estimation  
534 methods are generally not applicable to irregularly sampled time series, we have examined two  
535 broad types of estimation approaches and evaluated their performances against synthetic data  
536 with a wide range of prescribed  $\beta$  values and gap intervals that are representative of the sampling  
537 irregularity of real water-quality data.

538 The results of this work suggest several important messages. First, the results remind us of  
539 the risks in using interpolation for gap filling when examining auto-correlation, as the  
540 interpolation methods consistently under-estimate or over-estimate  $\beta$  under a wide range of  
541 prescribed  $\beta$  values and gap distributions. Second, the ~~long-established~~widely used Lomb-  
542 Scargle spectral method also consistently under-estimates  $\beta$ . Its modified form, using the 5%  
543 lowest frequencies for spectral slope estimation, has very poor precision, although the overall  
544 bias is small. Third, the wavelet method, coupled with an aliasing filter, has the smallest bias and  
545 root-mean-squared error among all methods for a wide range of prescribed  $\beta$  values and gap  
546 distributions, except for cases with small prescribed  $\beta$  values (*i.e.*, close to white noise) or small  
547  $\lambda$  values (*i.e.*, very skewed gap distributions). Thus, the wavelet method is recommended for  
548 estimating spectral slopes s in irregular time series until improved methods are developed. In this  
549 regard, future research should aim to develop an aliasing filter that is more applicable to irregular  
550 time series with very skewed gap intervals. Finally, all methods' performances depend strongly  
551 on the sampling irregularity in terms of both the skewness and mean of gap-interval lengths,  
552 highlighting that the accuracy and precision of each method are data-specific.

553 Overall, these results provide new contributions in terms of better understanding and  
554 quantification of the proposed methods' performances for estimating the strength of fractal  
555 scaling in irregularly sampled water-quality data. In addition, the work has provided an  
556 innovative and general approach for modeling sampling irregularity in water-quality records.  
557 Moreover, this work has proposed and demonstrated a generalizable framework for data  
558 simulation (with gaps) and  $\beta$  estimation, which can be readily applied ~~toward the evaluation of~~ to  
559 evaluate other methods that are not covered in this work. More generally, the findings and  
560 approaches may also be broadly applicable to irregularly sampled data in other scientific  
561 disciplines. Last but not least, we note that accurate quantification of fractal scaling in irregular

562 water-quality time series remains an unresolved challenge for the hydrologic community and for  
563 many other disciplines that must grapple with irregular sampling.

#### 564 **Data Availability**

565 River monitoring data used in this study are available through the U.S. Geological Survey  
566 National Water Information System (<http://doi.org/10.5066/F7P55KJN>) and the Heidelberg  
567 University's National Center for Water Quality Research.

#### 568 **Supporting Information**

569 Supporting information to this article is available online.

#### 570 **Competing Interests**

571 The authors declare that they have no conflict of interest.

#### 572 **Acknowledgements**

573 Zhang was supported by the Maryland Sea Grant through awards NA10OAR4170072 and  
574 NA14OAR1470090 and by the Maryland Water Resources Research Center through a graduate  
575 fellowship while he was a doctoral student at the Johns Hopkins University. Subsequent support to Zhang  
576 was provided by the USEPA under grant "EPA/CBP Technical Support 2017" (No. 07-5-230480).  
577 Harman's contribution to this work was supported by the National Science Foundation through grants  
578 CBET-1360415 and EAR-1344664. We thank Bill Ball (Johns Hopkins University) and Bob Hirsch (U.S.  
579 Geological Survey) for many useful discussions. This is contribution no. ~~xxxx to~~ 5449 of the University  
580 of Maryland Center for Environmental Science.

#### 581 **References**

- 582 Aubert, A. H., J. W. Kirchner, C. Gascuel-Oudou, M. Fauchoux, G. Gruau and P. Mérot, 2014. Fractal  
583 water quality fluctuations spanning the periodic table in an intensively farmed watershed.  
584 *Environ. Sci. Technol.* 48:930-937, DOI: 10.1021/es403723r.
- 585 Beran, J., 2010. Long-range dependence. *Wiley Interdiscip. Rev. Comput. Stat.* 2:26-35, DOI:  
586 10.1002/wics.52.
- 587 Beran, J., Y. Feng, S. Ghosh and R. Kulik, 2013. *Long-Memory Processes: Probabilistic Properties and*  
588 *Statistical Methods*. Berlin, Heidelberg, Springer Berlin Heidelberg, ISBN 978-3-642-35511-0

589 Boutahar, M., V. Marimoutou and L. Nouira, 2007. Estimation Methods of the Long Memory Parameter:  
590 Monte Carlo Analysis and Application. *J. Appl. Stat.* 34:261-301, DOI:  
591 10.1080/02664760601004874.

592 Box, G. E. P., G. M. Jenkins and G. C. Reinsel, 2008. *Time Series Analysis, Fourth Edition*. Hoboken, NJ,  
593 John Wiley & Sons, Inc., ISBN 9781118619193

594 Clarke, R. T., 2013. Calculating uncertainty in regional estimates of trend in streamflow with both serial  
595 and spatial correlations. *Water Resour. Res.* 49:7120-7125, DOI: 10.1002/wrcr.20465.

596 Cleveland, W. S., 1981. LOWESS: A program for smoothing scatterplots by robust locally weighted  
597 regression. *Am. Stat.* 35:54, DOI: 10.2307/2683591.

598 Cohn, T. A. and H. F. Lins, 2005. Nature's style: Naturally trendy. *Geophys. Res. Lett.* 32:L23402, DOI:  
599 10.1029/2005GL024476.

600 Constantine, W. and D. Percival, 2014. *fractal: Fractal Time Series Modeling and Analysis*,

601 Darken, P. F., C. E. Zipper, G. I. Holtzman and E. P. Smith, 2002. Serial correlation in water quality  
602 variables: Estimation and implications for trend analysis. *Water Resour. Res.* 38:1117, DOI:  
603 10.1029/2001WR001065.

604 Delignette-Muller, M. L. and C. Dutang, 2015. fitdistrplus: An R Package for Fitting Distributions. *J.*  
605 *Stat. Softw.* 64:1-34, DOI.

606 Ehsanzadeh, E. and K. Adamowski, 2010. Trends in timing of low stream flows in Canada: impact of  
607 autocorrelation and long-term persistence. *Hydrol. Process.* 24:970-980, DOI: 10.1002/hyp.7533.

608 Faticchi, S., S. M. Barbosa, E. Caporali and M. E. Silva, 2009. Deterministic versus stochastic trends:  
609 Detection and challenges. *J. Geophys. Res.* 114:D18121, DOI: 10.1029/2009JD011960.

610 Foster, G., 1996. Wavelets for period analysis of unevenly sampled time series. *Astron. J.* 112:1709-1729,  
611 DOI, <http://articles.adsabs.harvard.edu/full/1996AJ....112.1709F>.

612 Franzke, C., 2012a. Nonlinear Trends, Long-Range Dependence, and Climate Noise Properties of Surface  
613 Temperature. *J. Clim.* 25:4172-4183, DOI: 10.1175/JCLI-D-11-00293.1.

614 Franzke, C., 2012b. On the statistical significance of surface air temperature trends in the Eurasian Arctic  
615 region. *Geophys. Res. Lett.* 39:L23705, DOI: 10.1029/2012GL054244.

616 Godsey, S. E., W. Aas, T. A. Clair, H. A. de Wit, I. J. Fernandez, J. S. Kahl, I. A. Malcolm, C. Neal, M.  
617 Neal, S. J. Nelson, S. A. Norton, M. C. Palucis, B. L. Skjelkvåle, C. Soulsby, D. Tetzlaff and J. W.  
618 Kirchner, 2010. Generality of fractal 1/f scaling in catchment tracer time series, and its  
619 implications for catchment travel time distributions. *Hydrol. Process.* 24:1660-1671, DOI:  
620 10.1002/hyp.7677.

621 Graham, J., 2009. Missing Data Analysis: Making It Work in the Real World. *Annu. Rev. Psychol.* 60:549-  
622 576, DOI: 10.1146/annurev.psych.58.110405.085530.

623 Helsel, D. R. and R. M. Hirsch, 2002. Statistical Methods in Water Resources. *U.S. Geological Survey*  
624 *Techniques of Water-Resources Investigations Book 4, Chapter A3*. U.S. Geological Survey,  
625 Reston, VA, p. 522. <http://pubs.usgs.gov/twri/twri4a3/>.

626 Hirsch, R. M., R. B. Alexander and R. A. Smith, 1991. Selection of methods for the detection and  
627 estimation of trends in water quality. *Water Resour. Res.* 27:803-813, DOI: 10.1029/91WR00259.  
628

629 Hirsch, R.M., D.L. Moyer and S.A. Archfield, 2010. Weighted regressions on time, discharge, and season  
630 (WRTDS), with an application to Chesapeake Bay river inputs. *J. Am. Water Resour. Assoc.*  
631 46:857-880, DOI: 10.1111/j.1752-1688.2010.00482.x.

632 Hurst, H. E., 1951. Long-term storage capacity of reservoirs. *Trans. Amer. Soc. Civil Eng.* 116:770-808,  
633 DOI.

634 Khaliq, M. N., T. B. M. J. Ouarda and P. Gachon, 2009. Identification of temporal trends in annual and  
635 seasonal low flows occurring in Canadian rivers: The effect of short- and long-term persistence.  
636 *J. Hydro.* 369:183-197, DOI: 10.1016/j.jhydrol.2009.02.045.

637 Khaliq, M. N., T. B. M. J. Ouarda, P. Gachon and L. Sushama, 2008. Temporal evolution of low-flow  
638 regimes in Canadian rivers. *Water Resour. Res.* 44:W08436, DOI: 10.1029/2007WR006132.

639 Kirchner, J., 2005. Aliasing in  $1/f^\alpha$  noise spectra: Origins, consequences, and remedies. *Phys. Rev. E*  
640 71:066110-066110, DOI: 10.1103/PhysRevE.71.066110.

641 Kirchner, J. W., X. Feng and C. Neal, 2000. Fractal stream chemistry and its implications for contaminant  
642 transport in catchments. *Nature* 403:524-527, DOI: 10.1038/35000537.

643 Kirchner, J. W., X. Feng and C. Neal, 2001. Catchment-scale advection and dispersion as a mechanism  
644 for fractal scaling in stream tracer concentrations. *J. Hydro.* 254:82-101, DOI: 10.1016/s0022-  
645 1694(01)00487-5.

646 Kirchner, J. W. and C. Neal, 2013. Universal fractal scaling in stream chemistry and its implications for  
647 solute transport and water quality trend detection. *Proc. Natl. Acad. Sci. U. S. A.* 110:12213-  
648 12218, DOI: 10.1073/pnas.1304328110.

649 Kirchner, J. W. and A. Weil, 1998. No fractals in fossil extinction statistics. *Nature* 395:337-338, DOI:  
650 10.1038/26384.

651 Langland, M. J., J. D. Blomquist, D. L. Moyer and K. E. Hyer, 2012. Nutrient and suspended-sediment  
652 trends, loads, and yields and development of an indicator of streamwater quality at nontidal sites  
653 in the Chesapeake Bay watershed, 1985-2010. U.S. Geological Survey Scientific Investigations  
654 Report 2012-5093, Reston, VA, p. 26. <http://pubs.usgs.gov/sir/2012/5093/pdf/sir2012-5093.pdf>.

655 Lennartz, S. and A. Bunde, 2009. Trend evaluation in records with long-term memory: Application to  
656 global warming. *Geophys. Res. Lett.* 36:L16706, DOI: 10.1029/2009GL039516.



657 Lomb, N. R., 1976. Least-squares frequency analysis of unequally spaced data. *Astrophysics and Space*  
658 *Science* 39:447-462, DOI: 10.1007/BF00648343.

659 Montanari, A., R. Rosso and M. S. Taquq, 1997. Fractionally differenced ARIMA models applied to  
660 hydrologic time series: Identification, estimation, and simulation. *Water Resour. Res.* 33:1035-  
661 1044, DOI: 10.1029/97WR00043.

662 Montanari, A., R. Rosso and M. S. Taquq, 2000. A seasonal fractional ARIMA Model applied to the Nile  
663 River monthly flows at Aswan. *Water Resour. Res.* 36:1249-1259, DOI:  
664 10.1029/2000WR900012.

665 Montanari, A., M. S. Taquq and V. Teverovsky, 1999. Estimating long-range dependence in the presence  
666 of periodicity: An empirical study. *Math. Comput. Model.* 29:217-228, DOI: 10.1016/S0895-  
667 7177(99)00104-1.

668 National Center for Water Quality Research, 2015. Tributary Data Download. Accessed July 23, 2015,  
669 [https://www.heidelberg.edu/academics/research-and-centers/national-center-for-water-quality-](https://www.heidelberg.edu/academics/research-and-centers/national-center-for-water-quality-research/tributary-data-download)  
670 [research/tributary-data-download](https://www.heidelberg.edu/academics/research-and-centers/national-center-for-water-quality-research/tributary-data-download).

671 Noguchi, K., Y. R. Gel and C. R. Duguay, 2011. Bootstrap-based tests for trends in hydrological time  
672 series, with application to ice phenology data. *J. Hydro.* 410:150-161, DOI:  
673 10.1016/j.jhydrol.2011.09.008.

674 R Development Core Team, 2014. R: A language and environment for statistical computing. R Foundation  
675 for Statistical Computing, Vienna, Austria. ISBN 3900051070. <http://www.r-project.org>.

676 Rea, W., L. Oxley, M. Reale and J. Brown, 2009. Estimators for Long Range Dependence: An Empirical  
677 Study. *Electron. J. Stat.*, <http://arxiv.org/abs/0901.0762>, DOI.

678 Sang, Y.-F., Z. Wang and C. Liu, 2014. Comparison of the MK test and EMD method for trend  
679 identification in hydrological time series. *J. Hydro.* 510:293-298, DOI:  
680 10.1016/j.jhydrol.2013.12.039.

681 Scargle, J. D., 1982. Studies in Astronomical Time-Series Analysis. II. Statistical Aspects of Spectral-  
682 Analysis of Unevenly Spaced Data. *Astrophys. J.* 263:835-853, DOI: 10.1086/160554.

683 Stroe-Kunold, E., T. Stadnytska, J. Werner and S. Braun, 2009. Estimating long-range dependence in time  
684 series: an evaluation of estimators implemented in R. *Behav. Res. Methods* 41:909-923, DOI:  
685 10.3758/BRM.41.3.909.

686 Taquq, M. S., V. Teverovsky and W. Willinger, 1995. Estimators for long-range dependence: an empirical  
687 study. *Fractals*, <http://www.worldscientific.com/doi/abs/10.1142/S0218348X95000692>, DOI.

688 Wang, Z., 2013. cts: An R Package for Continuous Time Autoregressive Models via Kalman Filter. *J.*  
689 *Stat. Softw.* 53:1-19, DOI.

690 Witt, A. and B. D. Malamud, 2013. Quantification of Long-Range Persistence in Geophysical Time

691 Series: Conventional and Benchmark-Based Improvement Techniques. *Surv. Geophys.* 34:541-  
692 651, DOI: 10.1007/s10712-012-9217-8.

693 Yue, S., P. Pilon, B. Phinney and G. Cavadias, 2002. The influence of autocorrelation on the ability to  
694 detect trend in hydrological series. *Hydrol. Process.* 16:1807-1829, DOI: 10.1002/hyp.1095.

695 Zeileis, A. and G. Grothendieck, 2005. zoo: S3 Infrastructure for Regular and Irregular Time Series. *J.*  
696 *Stat. Softw.* 14:1-27, DOI.

697 Zetterqvist, L., 1991. Statistical Estimation and Interpretation of Trends in Water Quality Time Series.  
698 *Water Resour. Res.* 27:1637-1648, DOI: 10.1029/91wr00478.

699 Zhang, Q. and W. P. Ball, 2017. Improving Riverine Constituent Concentration and Flux Estimation by  
700 Accounting for Antecedent Discharge Conditions. *J. Hydro.* 547:387–402, DOI:  
701 10.1016/j.jhydrol.2016.12.052.

702 Zhang, Q., D. C. Brady, W. R. Boynton and W. P. Ball, 2015. Long-Term Trends of Nutrients and  
703 Sediment from the Nontidal Chesapeake Watershed: An Assessment of Progress by River and  
704 Season. *J. Am. Water Resour. Assoc.* 51:1534-1555, DOI: 10.1111/1752-1688.12327.

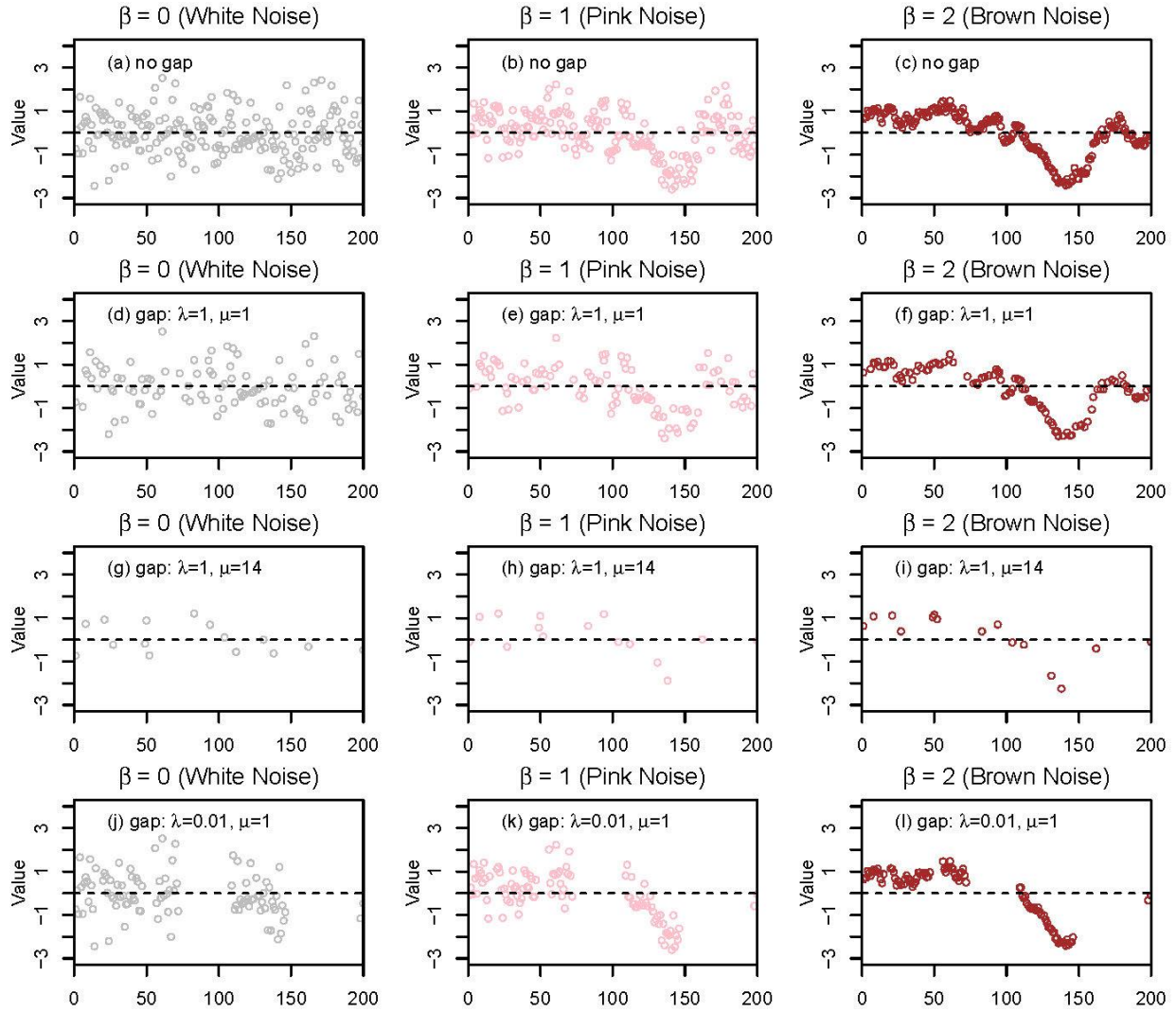
**Table 1.** Quantification of sampling irregularity for selected water-quality constituents at nine sites of the Chesapeake Bay River Input Monitoring program and six sites of the Lake Erie and Ohio tributary monitoring program. ( $\mu$ : mean parameter;  $\lambda$ : shape parameter estimated using maximum likelihood;  $\lambda'$ : shape parameter estimated using the direct approach (see **Section 2.2**).  $\Delta t_{average}$ : average gap interval;  $N$ : total number of samples.)

*I. Chesapeake Bay River Input Monitoring program*

Site ID	River and station name	Drainage area (mi <sup>2</sup> )	Total nitrogen (TN)					Total phosphorus (TP)				
			$\lambda$	$\lambda'$	$\mu$	$\Delta t_{average}$ (days)	$N$	$\lambda$	$\lambda'$	$\mu$	$\Delta t_{average}$ (days)	$N$
01578310	Susquehanna River at Conowingo, MD	27,100	0.8	1.1	13.5	14.5	876	0.8	1.0	13.4	14.4	881
01646580	Potomac River at Chain Bridge, Washington D.C.	11,600	0.9	0.6	9.5	10.5	1,385	1.1	1.0	24.4	25.4	579
02035000	James River at Cartersville, VA	6,260	0.8	1.0	13.9	14.9	960	0.8	1.1	13.7	14.7	974
01668000	Rappahannock River near Fredericksburg, VA	1,600	0.8	0.6	15.6	16.6	776	0.8	0.6	15.2	16.2	796
02041650	Appomattox River at Matoaca, VA	1,340	0.8	0.8	15.1	16.1	798	0.8	0.8	14.9	15.9	810
01673000	Pamunkey River near Hanover, VA	1,071	0.8	0.9	15.1	16.1	873	0.8	1.0	14.7	15.7	894
01674500	Mattaponi River near Beulahville, VA	601	0.7	0.9	14.3	15.3	810	0.8	0.9	14.2	15.2	820
01594440	Patuxent River at Bowie, MD	348	0.9	1.1	15.3	16.3	787	0.8	0.8	14.0	15.0	861
01491000	Choptank River near Greensboro, MD	113	1.2	1.5	19.6	20.6	680	1.1	1.0	20.5	21.5	690

*II. Lake Erie and Ohio tributary monitoring program*

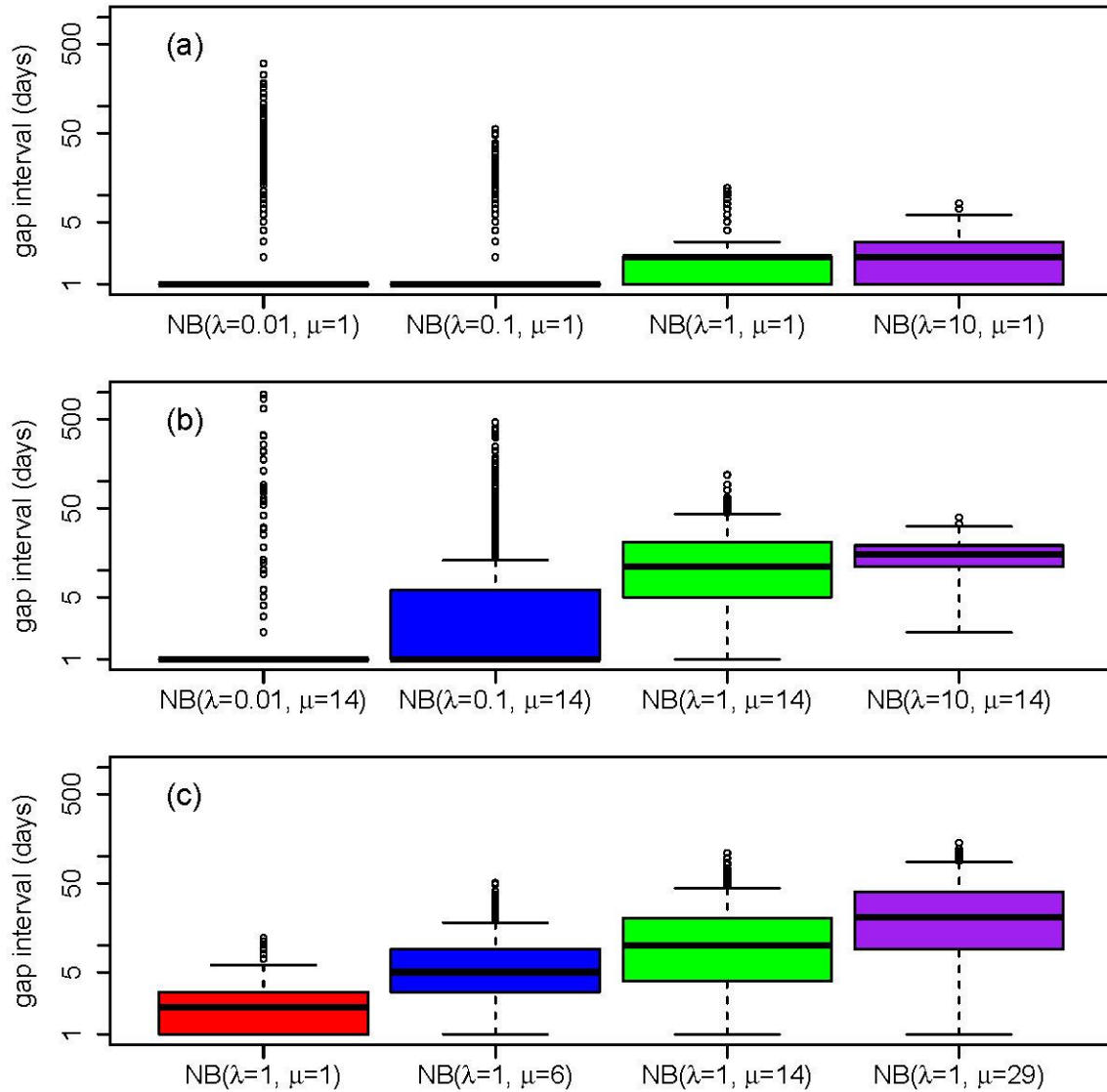
Site ID	River and station name	Drainage area (mi <sup>2</sup> )	Nitrate-plus-nitrite (NO <sub>x</sub> )					Total phosphorus (TP)				
			$\lambda$	$\lambda'$	$\mu$	$\Delta t_{average}$ (days)	$N$	$\lambda$	$\lambda'$	$\mu$	$\Delta t_{average}$ (days)	$N$
04193500	Maumee River at Waterville, OH	6,330	0.005	0.0003	0.19	1.19	9,101	0.005	0.0003	0.19	1.19	9,101
04198000	Sandusky River near Fremont, OH	1,253	0.01	0.003	0.22	1.22	9,641	0.01	0.003	0.22	1.22	9,655
04208000	Cuyahoga River at Independence, OH	708	0.007	0.006	0.13	1.13	7,421	0.007	0.006	0.13	1.13	7,426
04212100	Grand River near Painesville, OH	686	0.01	0.005	0.21	1.21	5,023	0.01	0.005	0.22	1.22	4,994
04197100	Honey Creek at Melmore, OH	149	0.007	0.005	0.06	1.06	9,914	0.007	0.005	0.06	1.06	9,914
04197170	Rock Creek at Tiffin, OH	34.6	0.007	0.008	0.06	1.06	8,422	0.007	0.008	0.06	1.06	8,440



705

706 **Figure 1.** Synthetic time series with 200 time steps for three representative fractal scaling  
 707 processes that correspond to white noise ( $\beta = 0$ ), pink noise ( $\beta = 1$ ), and Brown noise ( $\beta = 2$ ).

708 The 1<sup>st</sup> row shows the simulated time series without any gap. The three rows below show the  
 709 same time series as in the 1<sup>st</sup> row but with data gaps that were simulated using three different  
 710 negative binomial (NB) distributions, that is, 2<sup>nd</sup> row:  $\text{NB}(\lambda = 1, \mu = 1)$ ; 3<sup>rd</sup> row:  $\text{NB}(\lambda = 1, \mu =$   
 711  $14)$ ; 4<sup>th</sup> row:  $\text{NB}(\lambda = 0.01, \mu = 1)$ .

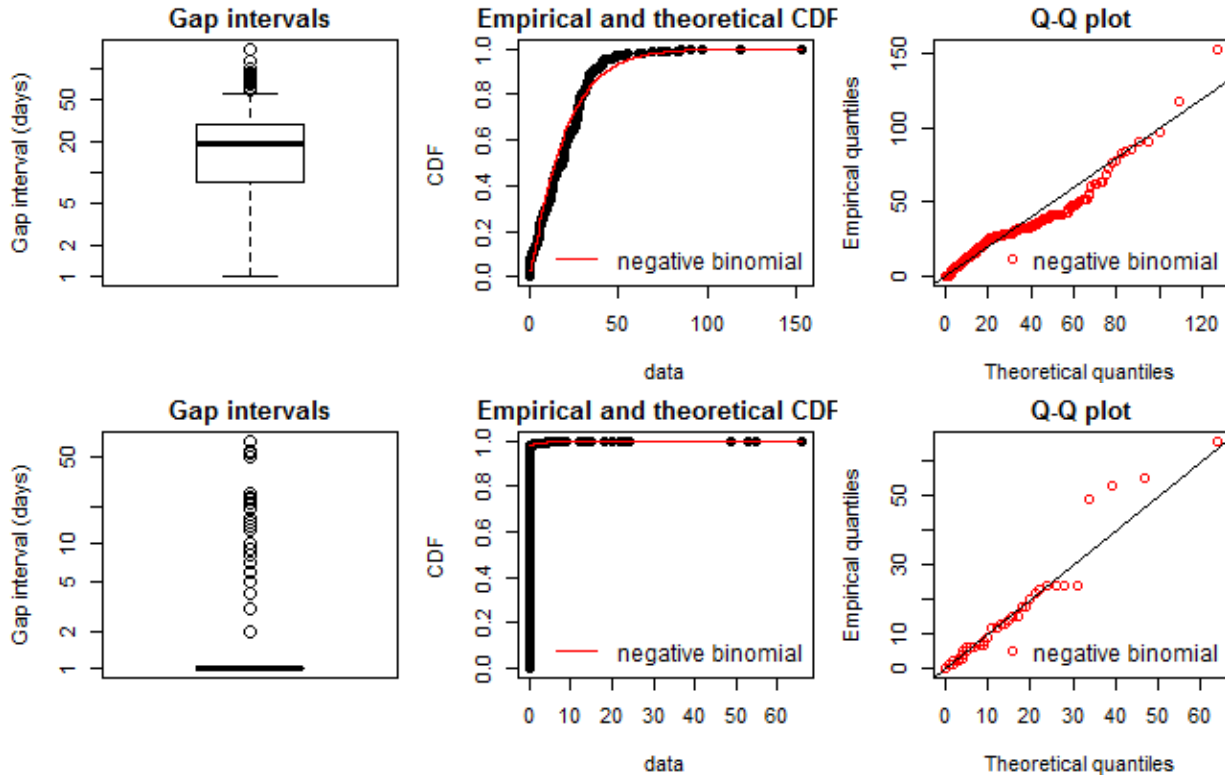


712

713 **Figure 2.** Examples of gap interval simulation using binomial distributions, NB (shape  $\lambda$ , mean

714  $\mu$ ). Simulation parameters:  $L = 9125$  days,  $\Delta t_{nominal} = 1$  day. The three panels show simulation

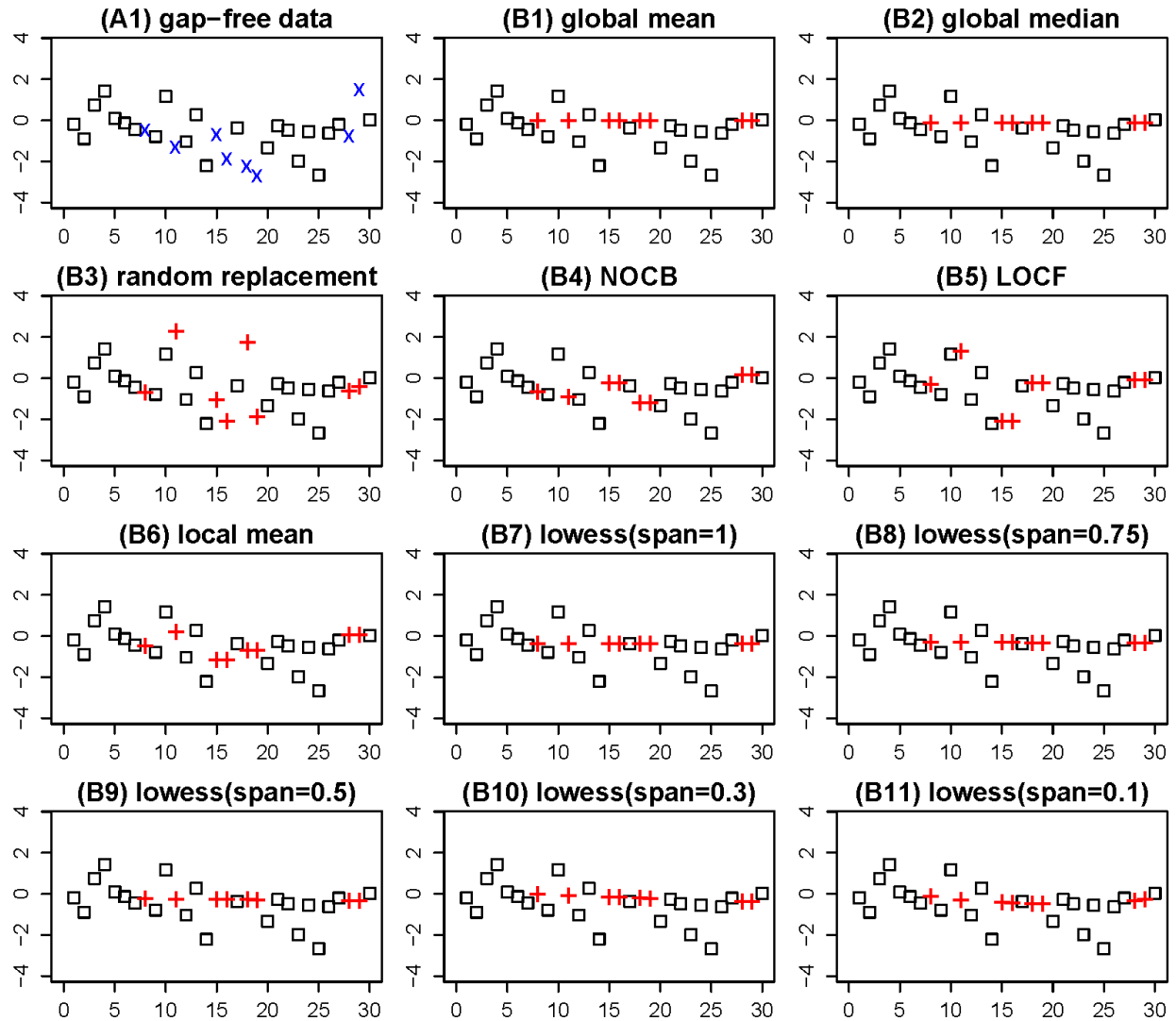
715 with fixed (a)  $\mu = 1$ , (b)  $\mu = 14$ , and (c)  $\lambda = 1$ . Note that  $\Delta t_{average}/\Delta t_{nominal} = \mu + 1$ .



716

717

718 **Figure 3.** Examples of quantified sampling irregularity with negative binomial (NB)  
 719 distributions: total nitrogen in Choptank River (top) and total phosphorus in Cuyahoga River  
 720 (bottom). Theoretical CDF and quantiles are based on the fitted NB distributions. See **Table 1**  
 721 for estimated mean and shape parameters.



722

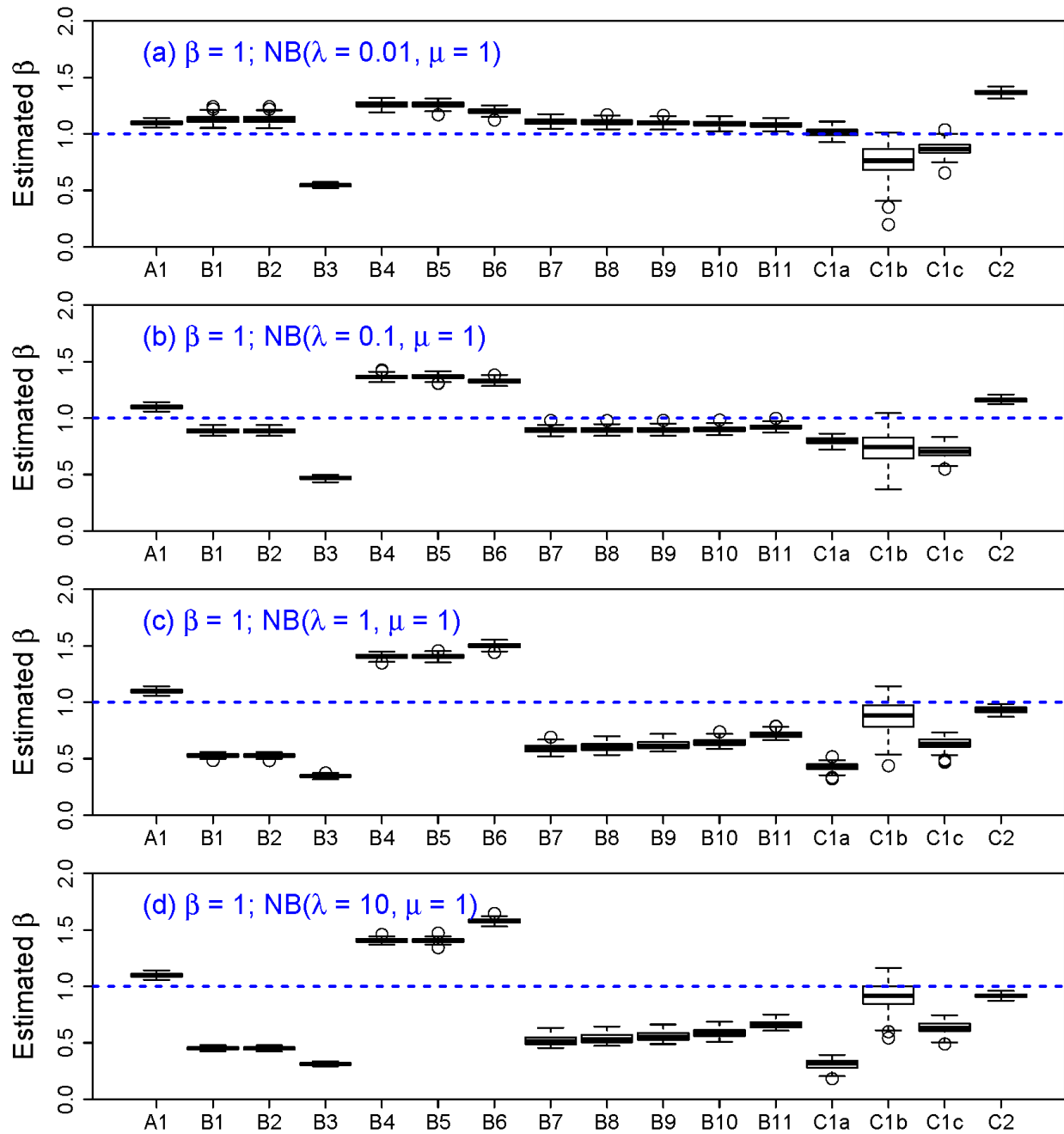
723

724

725

726

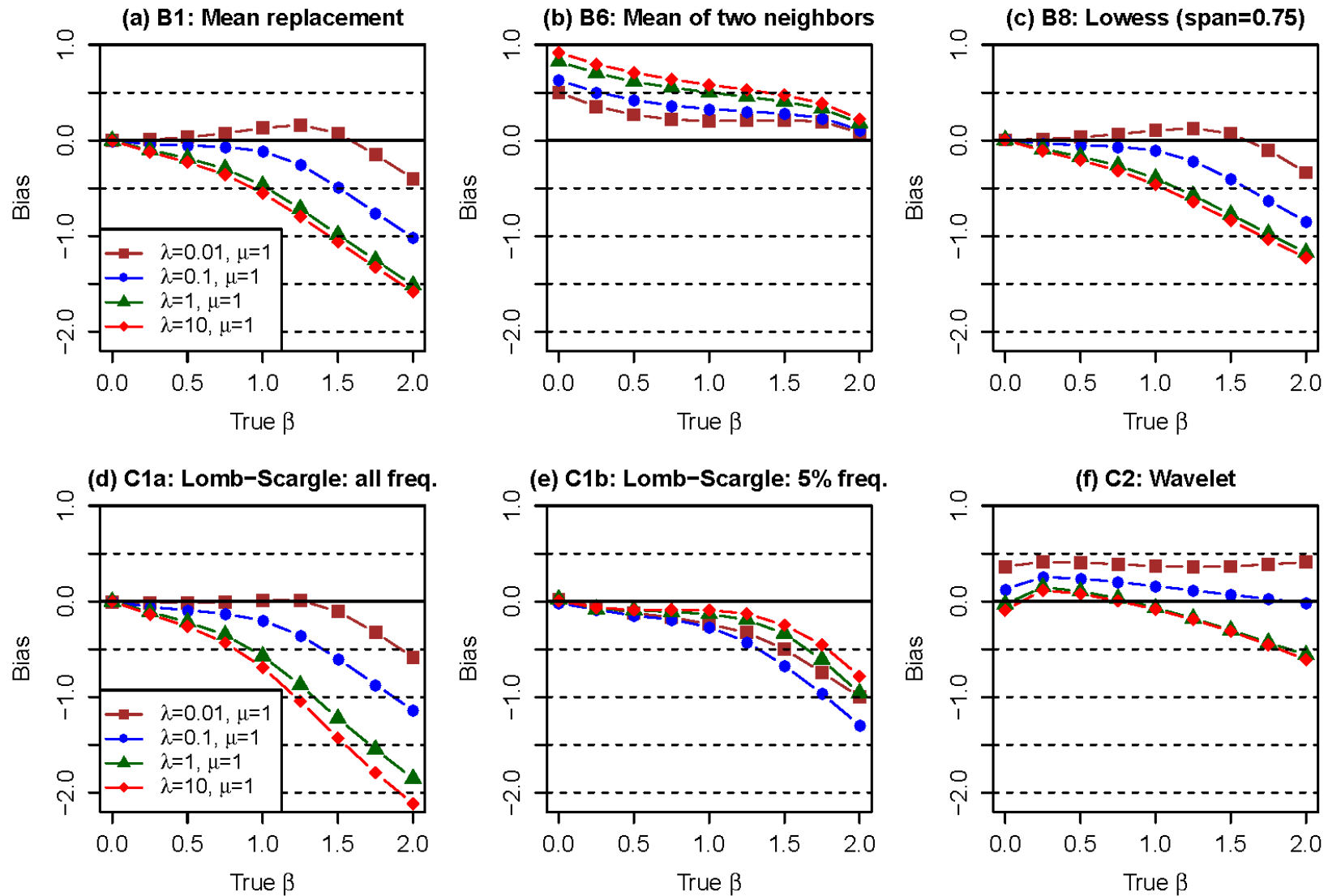
**Figure 4.** Illustration of the interpolation methods for gap filling. The gap-free data (A1) was simulated with a series length of 500, with the first 30 data shown. (x: omitted data for gap filling; +: interpolated data; NOCB: next observation carried backward; LOCF: last observation carried forward; lowess: locally weighted scatterplot smoothing.)



727

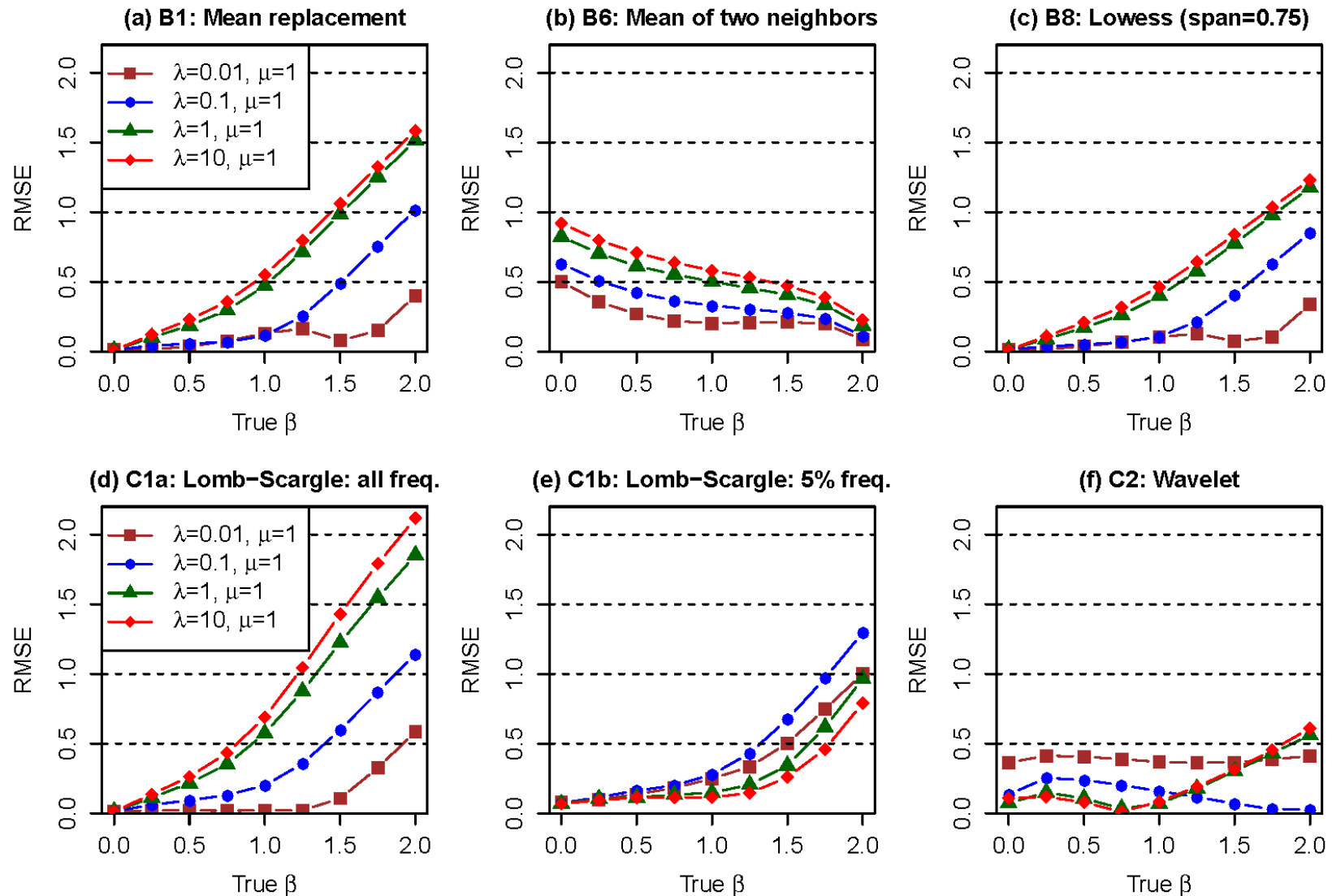
728 **Figure 5.** Comparison of bias in estimated spectral slope in irregular data that are simulated with  
 729 prescribed  $\beta = 1$  (100 replicates), series length of 9125, and gap intervals simulated with (a) NB  
 730 ( $\lambda = 0.01, \mu = 1$ ), (b) NB ( $\lambda = 0.1, \mu = 1$ ), (c) NB ( $\lambda = 1, \mu = 1$ ), and (d) NB ( $\lambda = 10, \mu = 1$ ). The  
 731 blue dashed lines indicate the true  $\beta$  value.





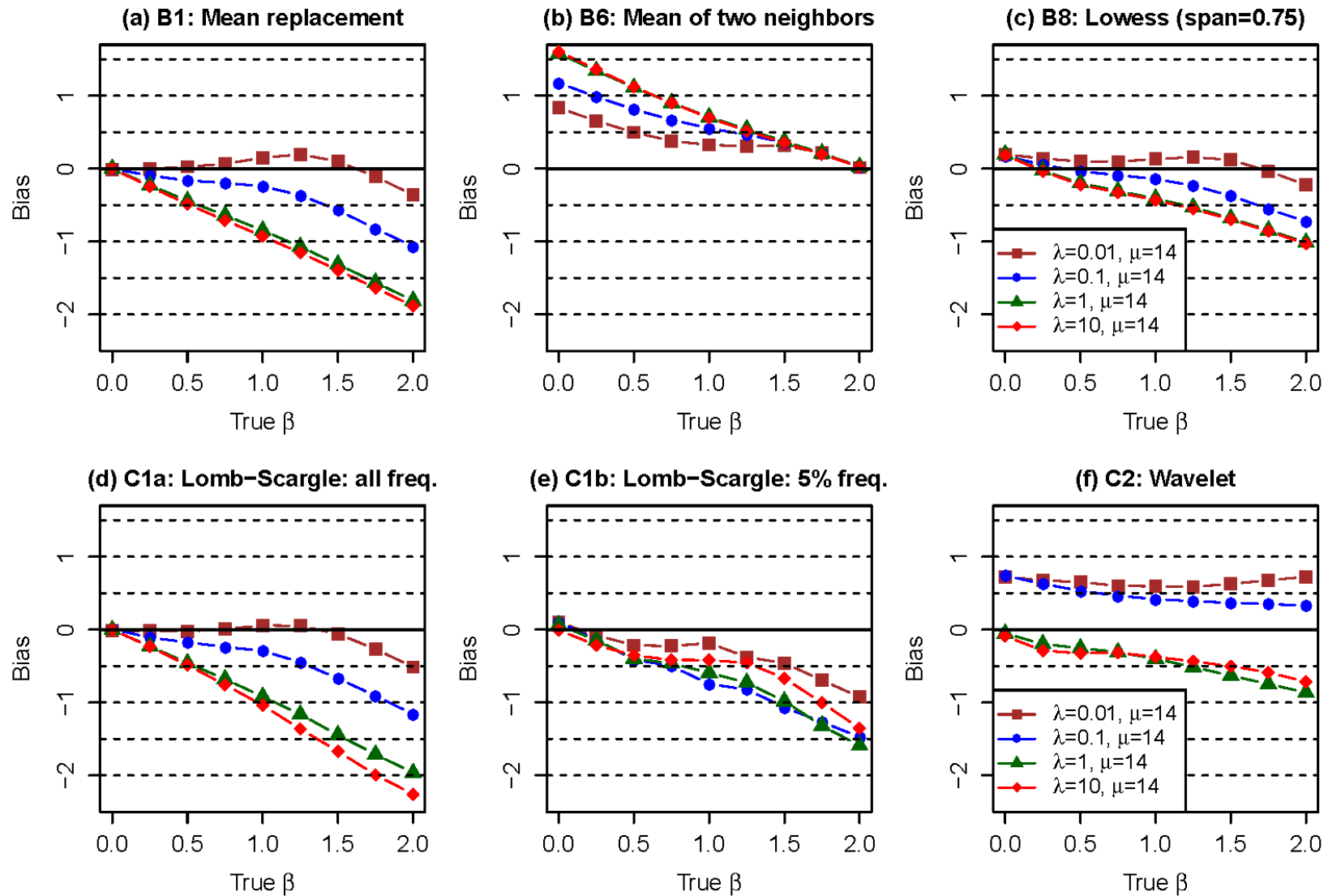
732

733 **Figure 6.** Comparison of bias in estimated spectral slope in irregular data that are simulated with varying prescribed  $\beta$  values (100  
 734 replicates), series length of 9125, and mean gap interval of 2 (*i.e.*,  $\mu = 1$ ).



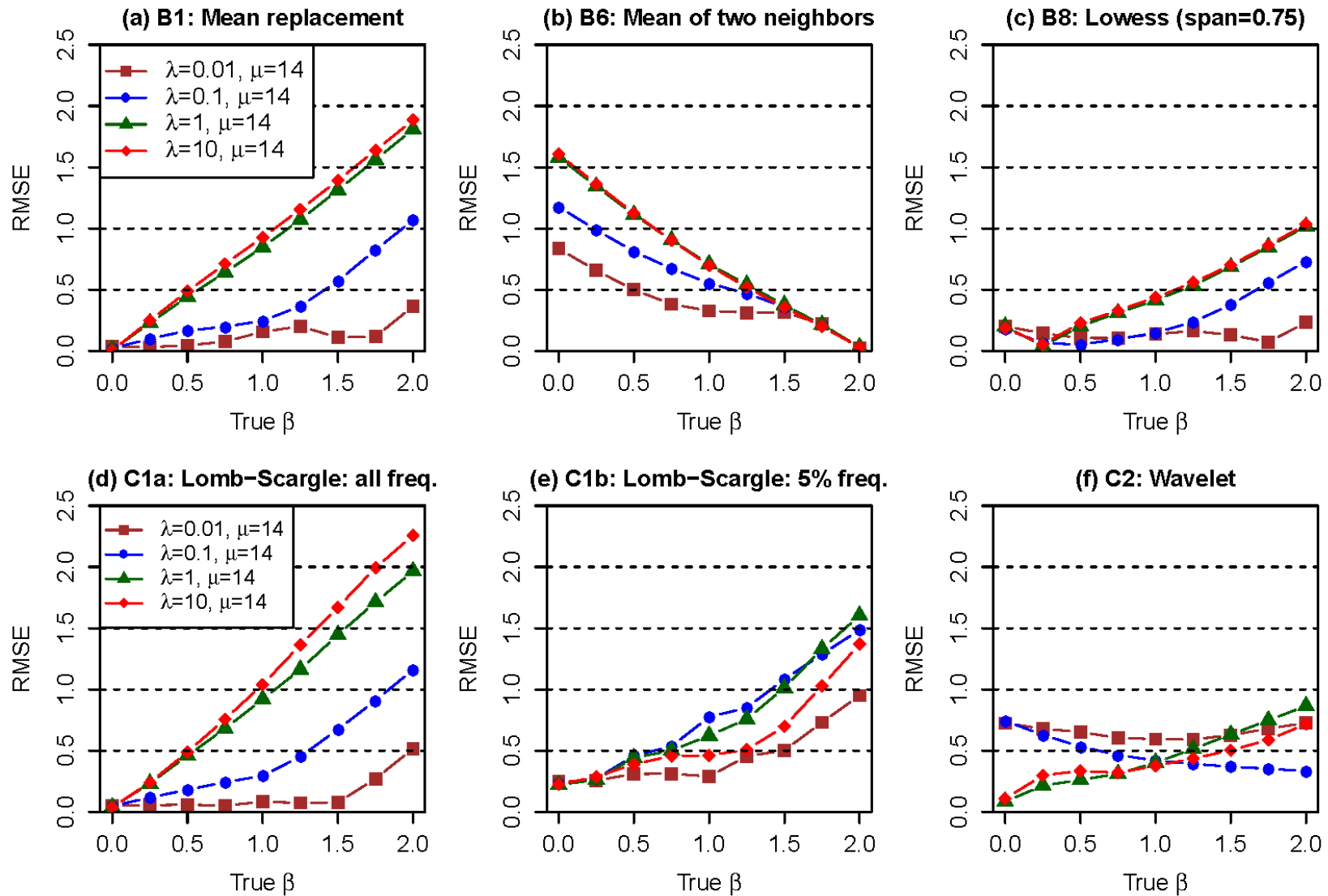
735

736 **Figure 7.** Comparison of root-mean-squared error (RMSE) in estimated spectral slope in irregular data that are simulated with varying  
 737 prescribed  $\beta$  values (100 replicates), series length of 9125, and mean gap interval of 2 (*i.e.*,  $\mu = 1$ ).



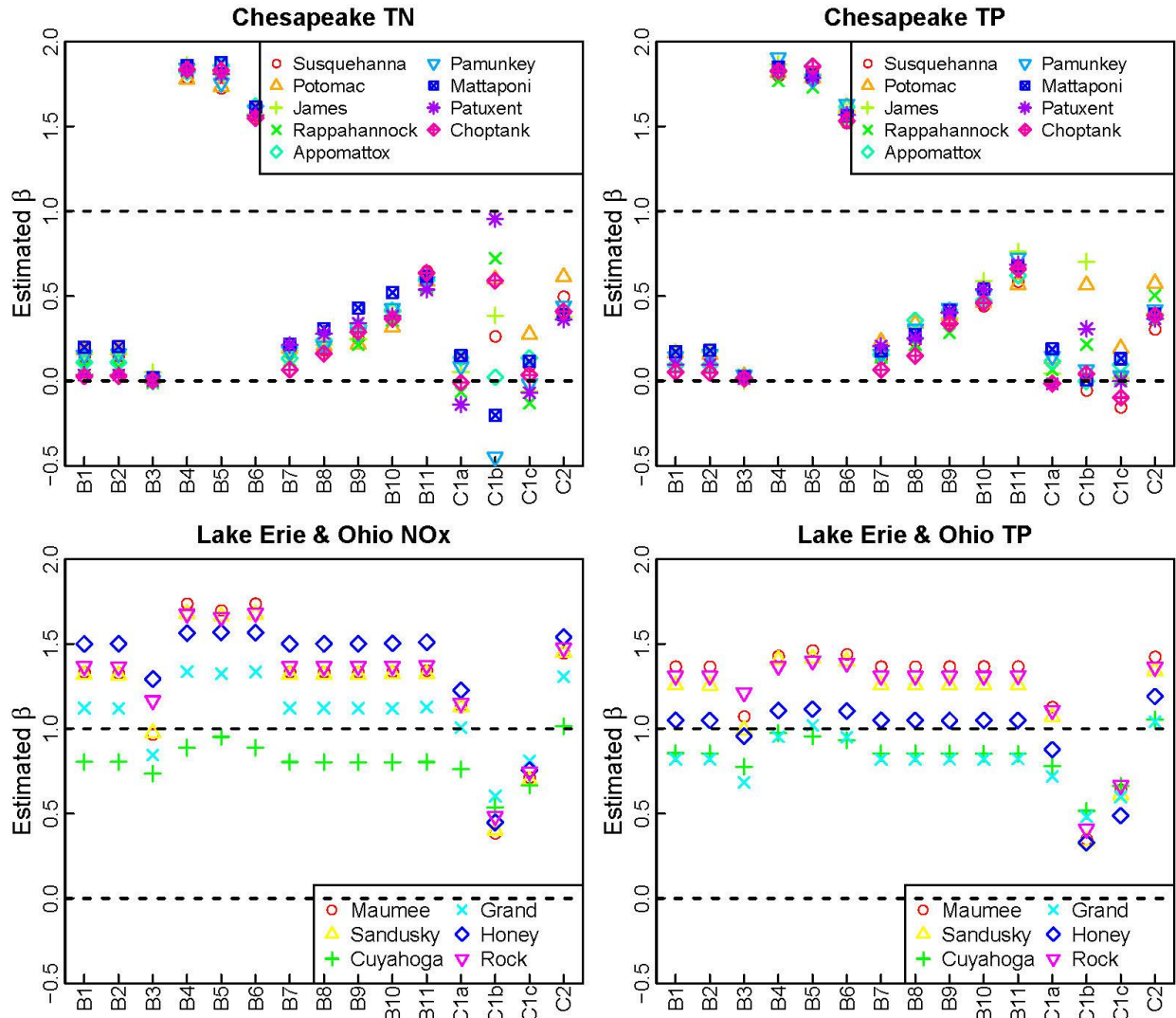
738

739 **Figure 8.** Comparison of bias in estimated spectral slope in irregular data that are simulated with varying prescribed  $\beta$  values (100  
 740 replicates), series length of 9125, and mean gap interval of 15 (*i.e.*,  $\mu = 14$ ).



741

742 **Figure 9.** Comparison of root-mean-squared error (RMSE) in estimated spectral slope in irregular data that are simulated with varying  
 743 prescribed  $\beta$  values (100 replicates), series length of 9125, and mean gap interval of 15 (*i.e.*,  $\mu = 14$ ).



744

745 **Figure 10.** Quantification of spectral slope in real water-quality data from the two regional  
 746 monitoring networks, as estimated using the set of examined methods. All estimations were  
 747 performed on concentration residuals (in natural log concentration units) after accounting for  
 748 effects of time, discharge, and season. The two dashed lines in each panel indicate white noise ( $\beta$   
 749 = 0) and pink (flicker) noise ( $\beta = 1$ ), respectively. See **Table 1** for site and data details.